Universität Stuttgart

INSTITUT FÜR AERODYNAMIK UND GASDYNAMIK

IAG

DIREKTOR: PROF. DR.-ING. EWALD KRÄMER

Pfaffenwaldring 21, 70550 Stuttgart, Tel. (0711) 685-63401, Fax 63402, email:kraemer@iag.uni-stuttgart.de

Design and Verification of an Airfoil with Trailing-Edge Flap and Unsteady Wind-Tunnel Tests

UPWIND WP1B3

TECHNICAL REPORT

Deliverable D3.8

Thorsten Lutz[1)]
Alexander Wolf[1)], Werner Würz[1)]
and
Jean-Guillaume Jérémiasz[2)]

January 14, 2011

[1)]Institute of Aerodynamics and Gas Dynamics
University of Stuttgart
Pfaffenwaldring 21
D-70550 Stuttgart, Germany

[2)]LM Wind Power Blades

Contents

1 Motivation and objective

One of the objectives of the European research project UPWIND is the investigation of passive and active load alleviation techniques for large wind turbines. These activities on future “smart rotors” are conducted in work package WP1B3. One part of theses activities was dedicated to the assessment of different approaches for load control. The requirements on a smart rotor in general were summarized in the UPPWIND report [Barlas2008-2] while Ref. [Wolf2010-2] gives some survey on flow control devices. The main objective of the present study is the design as well as the numerical and experimental verification of a new airfoil with active trailing-edge flap (TEF) which represents the UPWIND WP1B3 contribution of the Institute of Aerodynamics and Gas Dynamics (IAG), University of Stuttgart. The new airfoil shows a relative thickness of 18% and was designed specifically for the needs of active load alleviation with the requirements, the design goals and the freestream conditions derived for the outer blade region of the UPWIND 5MW reference turbine. During the airfoil design not only the aerodynamic characteristics were considered but also low trailing-edge noise emission was anticipated.

The experimental aerodynamic and aeroacoustic verification of the new airfoil in comparison to a NACA reference section was performed in the Laminar Wind Tunnel (LWT) of the IAG. The details of the measuring campaigns are documented in Refs. [Würz2008], [Wolf2009], [Wolf2010]. The wind tunnel tests were supplemented by steady and unsteady numerical investigations using CFD methods and by predictions of the emitted trailing-edge noise. A summary of the airfoil design and verification can be found in Ref. [Lutz2010].

The report is completed by a summary on unsteady experimental investigations on an airfoil with trailing-edge flap and with a mini-flapped performed by LM Wind Power in the LM wind tunnel. Furthermore the design of the experimental set-up used for these investigations is described.

2 Requirements for an airfoil with active flap

2.1 Introduction

Due to wind shear, turbulence, misalignment and blade-tower interaction the blade sections encounter significant angle-of-attack variations during operation that result in considerable lift changes. Active load control aims on the reduction of the load fluctuations. The active trailing-edge flap (TEF) is one of the load control concepts examined within the UPWIND project. This chapter discusses the design criteria and requirements for a dedicated airfoil with TEF that is adapted to this application. Such an airfoil was designed by the IAG (Institute of Aerodynamics and Gas Dynamics), University of Stuttgart within the WP1B3 activities. The new airfoil was designed for the application within the outer part of the UPWIND 5MW reference turbine [Langen2007] to replace the NACA 64-618 section of the baseline design. In order to validate the performance of the new design, wind tunnel tests were be performed at the Laminar Wind Tunnel of the IAG and compared to available test results for the NACA 64-418 test section [Hulskamp2008].

2.2 General design objectives

In general, airfoils for wind turbine application have to be designed for high lift to drag ratio L/D within the intended design regime of lift coefficient c_l, Reynolds- and Mach number (compare Sec. 2.3). Further, the maximum lift should not strongly exceed the upper design c_l but there should be some safety margin between upper design AoA and stall AoA and, finally, hard stall should be avoided. For airfoils with TEFs for load control additional criteria have to be considered. The objective of load control is that the airfoil lift variation caused by the changing AoA should be counteracted by adequate flap deflection. Therefore, high flap efficiency $\Delta c_l/\Delta\eta$ is anticipated, i.e. a small flap deflection shall provide a large impact on lift. Strong nonlinearities of the flap efficiency vs. deflection angle should be avoided with regard to the controller design. At the same time the drag or L/D penalty should be as small as possible. Because with optimum load control the lift variations of the blade section are compensated by the flap deflection, the drag for any flap deflection has to be considered always for the same target c_l. Previous investigations [Barlas2009] have shown that the application of conventional airfoils with active trailing-edge flaps may result in a power reduction in the order of 0.5~1% if the controller is optimized for load control solely.

Another design objective is the limitation the flap hinge moment and its gradient in order to minimize the requirements for the actuator and the actuation power. But also the impact of the flap deflection on the overall pitching moment of the airfoil should be small to limit the impact of the load control on the blade torsion. A positive flap deflection increases the pitch-down moment which results in a smaller AoA by increased aeroelastic blade twist. The intended lift increase is thus counteracted by the reduced AoA which finally lowers the flap efficiency.

Numerical investigations by Troldborg [Troldborg2005] have shown that a flap of 10% chord represents a good compromise between efficiency and moment requirements. A smaller flap chord is advantageous with regard to the flap hinge moment but has a higher drag penalty for a certain Δc_l and provides a smaller Δc_l reserve. In his CFD simulations with prescribed pitching and flapping a 10% flap has shown to provide sufficient impact on lift for flap deflections within $\eta = \pm 10°$. Lackner and van Kuik [Lackner2009] performed aeroelastic simulations for a 5MW wind turbine and examined the load reduction potential by means of active TEFs. They found that for a 10% flap a deflection range of ±10° is sufficient for efficient load control. Comparable simulations were performed by Barlas and

van Kuik for the UPWIND 5MW reference turbine [Barlas2009]. They also concluded that a 10% flap and a deflection range of ±10° is sufficient for load control purposes but some Δc_l reserve for a deflection up to ±15° would be desirable for extreme conditions. A 10% flap chord is therefore considered as adequate and is chosen for the present airfoil design. A NACA 64-418 airfoil that was wind-tunnel tested in detail as well as the NACA 64-618 which represents the baseline section in the outer part of the UPWIND turbine will serve as reference airfoils to assess the characteristics of the new design.

In principle unsteady aerodynamic effects occur when a TEF is used for load control. Depending on the magnitude of the reduced frequency *k* a phase shift, hysteresis effects and a decreasing impact on the flap efficiency results. As described by Barlas [Barlas2008-2] the reduction of the flap efficiency, however, is expected to be smaller than the reduction of the lift curve slope of the baseline airfoil due to pitching. Lackner and van Kuik [Lackner2009] analyzed the flap motion required for load control. They found that most of the energy of the flapping motion for the considered turbine is around $k \approx 0.025$. This is lower than k=0.05 which is considered as a typical value where unsteady effects start to noticeably affect the aerodynamics. However also higher reduced frequencies can occur which are in the unsteady region. In the design process unsteady effects are not considered but will be analyzed by CFD studies on the resulting new design (see Sec. 3.4).

Beside these aerodynamic design objectives the airfoil should be designed with regard to minimize the trailing-edge noise as the outboard blade section dominates the turbine flow-induced overall noise emission. In particular a low A-weighted noise level within the design c_l regime is anticipated. The consideration of noise issues is an important criterion in the design of airfoils for onshore wind turbines. For an airfoil with TEF this is especially true because the flap deflection introduces local gradients in the pressure distribution that have an impact on the noise relevant boundary-layer properties and can cause separation which results in a significant noise increase.

2.3 Design conditions

The new airfoil was designed for the outer part of the UPWIND reference turbine to replace the 18% NACA 64-618 section. This baseline airfoil is being applied between 44.5m (70.6% R) and the tip at 63m blade radius [Langen2007]. The design conditions are derived from the outcome of Bladed GH aeroelastic simulations of the reference turbine performed by Barlas within the UPWIND project [Barlas2008]. In these simulations three different wind speeds were considered, namely 8m/s, 11.4m/s and 18 m/s, whereas yaw angles of 0, 15 and 35° were examined. A reference turbulence intensity of 14% according to IEC standard was chosen. For these conditions Ref. [Barlas2008] documents the variation of the AoA, the onset flow velocity and the lift coefficient for three different radius positions (r=47.15m, 54.66m and 60.13m). To define the main design condition for the new airfoil the mean values as resulting for r=54.66m at zero yaw angle and wind speeds below rated power (8m/s and 11.4m/s) were chosen. Assuming atmospheric standard conditions this gives:

Design condition #1: $Re=4.5 \cdot 10^6$, Ma=0.165, c_l=0.7 (0.4~1.2)

The design lift range c_l=0.4~1.2 corresponds to the c_l-variations that have shown up in the Bladed simulations for this radius position at wind speeds of 8m/s and 11.4m/s taking all examined yaw angles (ψ=0/15/35°) into account. These simulations suggest an average design lift coefficient of $c_l \approx 0.7$ which is quite small and can be attributed to sub-optimal blade design and AoA setting. It was therefore decided to focus on a higher design lift

coefficient of $c_l \approx 1.0$ for the new airfoil design but to keep the smaller target c_l in mind.

To define the upper and lower boundaries of the Reynolds number regime the minimum and maximum *Re* for all three radius positions, wind speeds of 8m/s and 11.4m/s and all three yaw angles (ψ=0/15/35°) were extracted and rounded. This defines the subsequent secondary design points:

Design condition #2: $Re=12 \cdot 10^6$, Ma=0.19
Design condition #3: $Re=1.0 \cdot 10^6$, Ma=0.18

This covers a very broad Reynolds number regime and some loss of performance will have to be accepted at the boundaries in favour of higher performance at design conditions #1 & #2. It should be mentioned that the low Reynolds number of $Re=1.0 \cdot 10^6$ occurs at the very tip of the blade where the chord is already very small.
Finally it is anticipated that the new airfoil shows no deterioration of performance at wind-tunnel conditions as these tests will be used to validate the calculations and to assess the airfoil. This gives the fourth condition to be considered in the airfoil design:

Design condition #4: c=0.6m, $Re=2.5 \cdot 10^6$, Ma=0.18

First of all, the airfoil shall be designed for maximum performance at natural boundary-layer transition, i.e. for clean blades without surface imperfections. But also forced transition near the leading edge shall be considered to simulate the situation when the blades are contaminated by dirt, insects or erosion. To consider the tripped condition is most important because a fully turbulent boundary layer can overcome less adverse pressure gradient and premature flow separation occurs. A flap deflection increases the adverse pressure gradient locally and augments the risk of flow separation. As a consequence the flap efficiency decreases and drag penalty as well as noise emission increase. To prevent boundary-layer separation for tripped conditions and maximum flap deflection represents a challenge for the airfoil design.

2.4 Summary of design criteria and constraints

Geometry

- relative airfoil thickness 18%
- airfoil thickness at the flap hinge not too small to enable housing of the actuators
- rigid flap of 10% chord
- flap hinge midway between upper and lower surface

Aerodynamics

- minimize drag for the design conditions discussed in Sec 2.3
- ensure high L/D and smooth L/D distribution around main design lift coefficient c_l=1.0 and c_l=0.7 also with flap deflection
- avoid L/D degradation in case of flap deflection compared to the baseline airfoil
- design for natural transition, check for tripped conditions
- maximize flap efficiency ($\Delta c_l/\Delta\eta$) at least till $\eta=\pm10°$ with some Δc_l reserve up to $\eta=\pm15°$
- avoid strong nonlinearities in the behaviour of the flap efficiency vs. deflection angle
- avoid flow separation within the design range also for deflected flap and tripped conditions
- minimize flap hinge moment $c_{m,\,flap}$ or gradient of the flap hinge moment $\Delta c_{m,\,flap}/\Delta\eta$
- limit impact of flap deflection on airfoil moment gradient $\Delta c_m/\Delta\eta$
- limit $c_{l,\,max} - c_{l,\,design}$
- no consideration of unsteady effects during the airfoil design

Aeroacoustics

- Minimize A-weigthed overall sound pressure level of the trailing edge noise for the baseline airfoil within the above design conditions
- Minimize noise penalty in case of flap deflection

3 Design of an airfoil with active flap

3.1 Numerical methods

Design methods

For the combined aerodynamic and acoustic design and analysis of airfoil sections different numerical tools are available at the institute. For the design and the basic aerodynamic analysis the well established XFOIL code [Drela89] is applied. The method is based on a coupled panel boundary-layer procedure which offers inverse, mixed-inverse design or direct analysis capabilities for single-element airfoils. The peculiarity of this method is that the governing equation for the outer-flow computation is directly coupled with the integral boundary-layer equations and simultaneously solved taking the boundary-layer displacement-effect into account. The implemented first order integral boundary-layer method is based on a numerical integration of the integral momentum and energy equation. For turbulent flows an additional lag-equation is solved which accounts for non-equilibrium effects. For transition prediction XFOIL uses a simplified e^n envelope method. To enable a more accurate and consistent prediction of the laminar to turbulent transition location, a complete e^n transition criterion was linked to XFOIL. To maximize the computational efficiency a data-base approach is implemented supplementary to a Orr-Sommerfeld solver.

To enable an aeroacoustic airfoil design, numerical optimization or analysis, a module for the trailing-edge noise prediction was being implemented and linked to the XFOIL airfoil analysis code in the frame of the past European SIROCCO project [Lutz2004], [Lutz2005], [Lutz2006], [Lutz2007]. This tool is routinely applied at the IAG to the combined aerodynamic and aeroacoustic design of low-noise high-performance airfoil sections for wind-turbine applications. The noise prediction model is based on theories by Blake [Blake1986], Chandiramani [Chandiramani1974] and Parchen [Parchen1998] and is commonly referred as TNO-TPD scheme. With this approach the unsteady surface pressure fluctuations as induced by the convecting turbulent eddies in the boundary layer are described by a wave-number frequency spectrum. The associated far-field noise emission is determined by evaluating the diffraction integral for a semi-infinite flat plate according to the model by Chandiramani. The model gives the spectrum of the far-field noise for a specified observer distance without account for directivity. As input the model requires the mean boundary-layer profile in the vicinity of the trailing edge along with the wall normal distributions of the vertical integral length scale and the rms value of the autocorrelation of the turbulent vertical velocity fluctuations. Two variants have been implemented [Kamruzzaman2010-3], [Lutz2007]. The Xnoise variant determines the input parameters from the integral boundary-layer properties provided by XFOIL while in the XEnoise version the required noise source terms are calculated by the Finite-Difference boundary-layer code EDDYBL, developed by Wilcox [Wilcox1998]. In the present study XEnoise was used. The initial and the boundary conditions for the EDDYBL analyses were determined by a preceeding XFOIL calculation.

As previous investigations [Lutz2007], [Kamruzzaman2010-3], [Kamruzzaman2011] have shown that anisotropy effects have an important impact on the trailing-edge noise the Wilcox stress-ω turbulence model was chosen in the present study. This model provides the complete REYNOLDS-stress tensor and thus the anisotropy of the velocity fluctuations but not of the length scales. In the present study a semi-empirical scaling law was used to determine the required vertical length scale Λ_2 from the predicted scalar turbulence scale [Lutz2007]. The scaling law was derived based on detailed boundary-layer measurements

in the institute's Laminar Wind Tunnel that were performed for different airfoil sections at several onset flow conditions.

Analyses methods

For aerodynamic analyses of airfoils and complete wind turbines the CFD code FLOWer [Kroll2002] is applied at the IAG. FLOWer solves the compressible Reynolds- averaged Navier-Stokes equations in integral form. A cell-centered based finite-volume formulation on block-stuctured grids was utilized for the present calculations. The convective fluxes of the main equations were discretized in space applying a second-order central scheme with a blend of second- and fourth-order artificial damping terms, whereas diffusive fluxes were discretized purely central. The turbulence equations were discretized by a flux difference first-order upwind scheme. Time integration to steady state for the main equations was accomplished by an explicit five-stage Runge-Kutta scheme with local time stepping, where convergence was accelerated by a multigrid method on three grid levels with implicite residual smoothing. The source-term dominated turbulence equations were integrated in time using a diagonal dominant alternating direction implicite (DDADI) scheme on the finest grid level at very high CFL-numbers. In the present study the Menter Shear-Stress-Transport model was applied.

To enable an automated generation of dedicated structured grids a library of scripts has been developed at the institute [Meister2009], [Meister2010] for the commercial mesh generators IGG and Gridgen respectively. The scripts enable the meshing of airfoils, 3D blades and wind rotors including nacelle. The surface geometry of the considered configurations can easily be modified which enables short turn-around times qualifying the approach to be used in a design process. The discretization, boundary-layer resolution and far-field distance can be controlled by simple user inputs. In Refs. [Meister2009], [Meister2010] this RANS-based aerodynamic process chain is described in more detail along with application examples.

The noise prediction model described above has been substantially extended at the IAG and coupled to the RANS code FLOWer to enable airfoil trailing-edge noise prediction in the analysis process. The extensions are dedicated to the physically consistent consideration of turbulence anisotropy effects based on standard output from one- or two-equation as well as Reynolds stress turbulence models. The theoretical background of the noise prediction scheme denoted Rnoise is described in Refs. [Kamruzzaman2007], [Kamruzzaman2008], [Kamruzzaman2010-1], [Kamruzzaman2010-2], [Kamruzzaman2010-2], [Kamruzzaman2010-3], [Kamruzzaman2011.

3.2 Impact of rigid trailing-edge on noise emission

Prior to the airfoil design numerical studies on the impact of flap deflections on the boundary-layer development [Lutz2007-2] and the trailing-edge noise emission [Lutz2007-3] were performed. In the acoustic study the NACA 64_3-418 airfoil was considered with a) a continuous camber variation b) a rigid flap of 20% chord and c) a rigid flap of 10% chord. Because a 10% flap has shown to be sufficient for load alleviation the results for this configuration will be summarized subsequently.

First of all aerodynamic analyses were performed for different flap settings. Fig. 1 depicts the results for a typical Reynolds number of $Re = 4 \cdot 10^6$, an angle of attack of $\alpha=4^o$ and natural transition. The left picture shows the predicted drag vs. lift coefficient c_l. For the baseline airfoil α was varied whereas for the adaptive airfoils the angle-of-attack was kept

constant. The lift variation was achieved by a continuous camber variation or a flap deflection respectively. On the right hand picture of Fig. 1 the corresponding A-weighted overall noise levels are given for a standard observer distance and wetted trailing edge length. It is obvious that a positive flap deflection or an increase of the airfoil camber reduces the drag compared to the baseline airfoil for lift coefficients higher than the reference angle-of-attack. At the same time a noise reduction can be observed. The situation is different for smaller lift coefficients where for the present airfoil and freestream conditions a decrease of the AoA is more advantageous compared to a de-cambering without AoA variation. This shows that for every lift coefficient an appropriate combination of angle-of-attack and flap deflection has to be chosen. Noteworthy, the smaller flap yields a higher noise reduction for higher c_l values than the larger flap or the camber variation respectively. For small c_l the situation is vice versa. It is therefore important to carefully consider the intended flap size and its impact on noise emission during the airfoil design phase. Fig. 2 depicts the corresponding results for the tripped case. The same qualitative behaviour can be observed as discussed for natural transition. In conclusion the application of a rigid trailing edge flap for load control must not have a negative impact on the noise emission. In fact beside performance improvement the noise could be reduced if an optimum combination of angle-of-attack and flap setting is chosen.

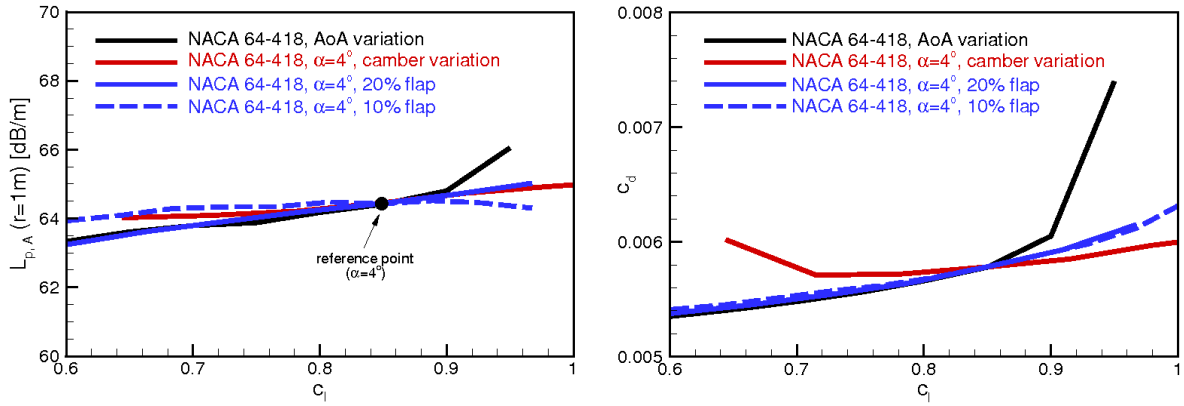

Fig. 1 Calculated impact of camber variation and flap deflection on airfoil drag (left figure) and noise (right figure), U_∞=60m/s, c=1m, Re=4x10^6, natural transition (n=9).

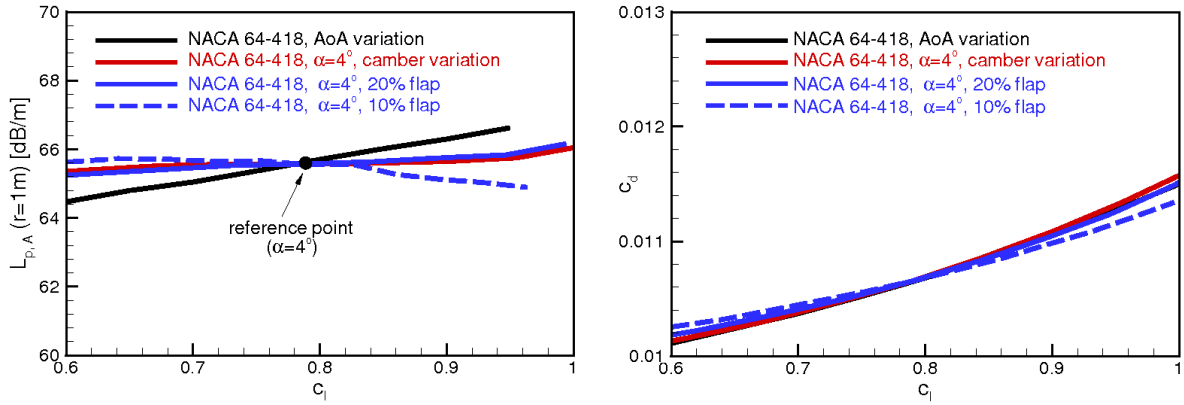

Fig. 2 Calculated impact of camber variation and flap deflection on airfoil drag (left figure) and noise (right figure), U_∞=60m/s, c=1m, Re=4x10^6, forced transition (5% chord on upper and lower side).

3.3 Design and numerical analysis of the new airfoil

The new airfoil was designed making use of XFOIL's mixed-inverse design capability. Besides the polar calculation for the above design conditions the flap efficiency, flap hinge moment and trailing-edge noise emission were analyzed for each design step and various flap deflection angles. To predict the transition location a full e^n method that calculates the frequency dependent TS amplification was linked to XFOIL. The turbulent boundary-layer trailing-edge interaction noise (TBL-TE) was determined by the institute's noise prediction scheme XEnoise (compare Sec. 3.1). For selected intermediate designs RANS analyses using different turbulence models were performed to check for separation tendency.

The shape and the inviscid pressure distribution of the final airfoil TL 190-82 are given in Fig. 3. The airfoil shows long regions of favourable pressure gradient in particular on the lower side in order to delay transition also for the highest design Reynolds number. Smooth transition ramps were introduced on both sides to avoid laminar separation bubbles at low Re within the design c_l regime. The transition ramps were designed specifically for the local Reynolds number region of interest. The airfoil features slightly concave pressure recovery regions on both sides shaped to reduce turbulent friction drag without corrupting the stall behaviour. Care was taken to limit the aft loading in order to reduce the airfoil moment and in particular the flap hinge moment. The suction side pressure distribution shows a distinct dip at the flap hinge position (90% chord). By this, separation is delayed for larger flap down deflection resulting in a continuous distribution and a broad range of high flap efficiency (compare Fig. 7). On the suction side an adverse pressure gradient downstream of the hinge point was avoided to reduce the tendency for noise increasing trailing-edge separation for flap down situations.

Fig. 4 shows the polars for the main design Reynolds number $Re = 4.5 \cdot 10^6$ and natural transition (critical amplification factor n=9) as predicted by the XFOIL code in combination with the full e^n transition criterion. Three different deflection angles of the 10% flap were analyzed, namely η=-10°, 0° and +10°. In addition the results for the tripped case (forced transition at x_{tr}/c=0.05 on suction and pressure side) are depicted in Fig. 5. In general the new airfoil shows good aerodynamic performance with the laminar bucket corresponding to the design lift regime, no obvious impact of separation (bubbles) and acceptable stall characteristics. The improvements compared to the NACA reference airfoil for natural transition are visualized in Fig. 6.

Fig. 7 finally depicts the most important results with respect to the applicability of the new airfoil for load control by means of active TEFs. To derive these results the AoA of the airfoil with neutral flap deflection was varied. The resulting c_l regime is given on the horizontal axes. The range covers the design c_l range specified above. The graphs, however, give the performance for a flap deflection chosen such that the resulting lift is always c_l=1.0, independent of the AoA. Thus, according to the principle of load control the flap exactly compensates the lift variations due to varying freestream angles seen by the blade section.

The upper left picture shows the drag distribution ($Re = 4.5 \cdot 10^6$, natural transition) of the new airfoil compared to the reference section. It is obvious that the new design shows smaller drag over the whole lift region and an enlarged low drag range. The upper right picture shows the predicted trailing-edge noise. The new airfoil shows lower noise emission except for a small c_l regime where both airfoils have comparable performance. As can be seen from the lower left picture the flap efficiency could be significantly improved with the new design, the range of high efficiency is considerably broadened. Finally the flap hinge moment could also slightly reduced compared to the NACA reference

section (lower right picture).

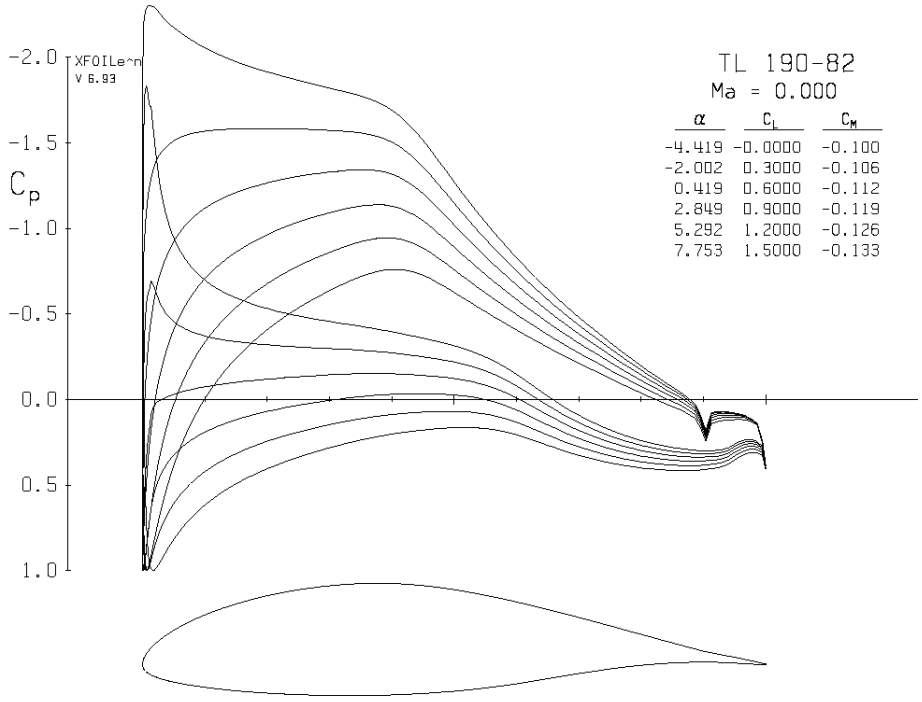

Fig. 3 Inviscid pressure distribution of the new airfoil with TEF

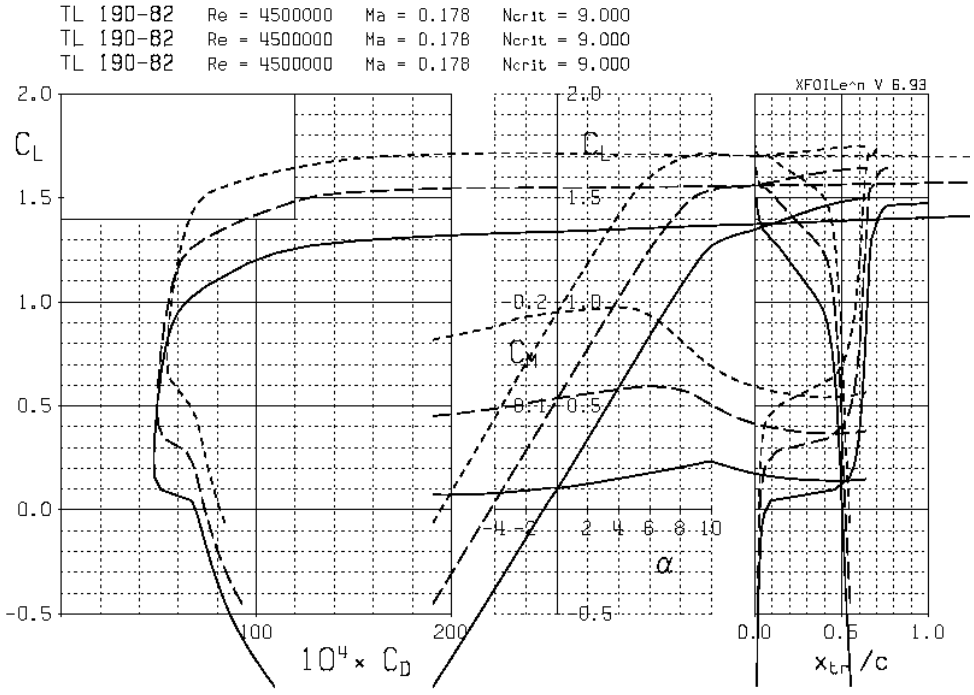

Fig. 4 Predicted polars of the new airfoil for η=-10°/0°/+10° (n=9)

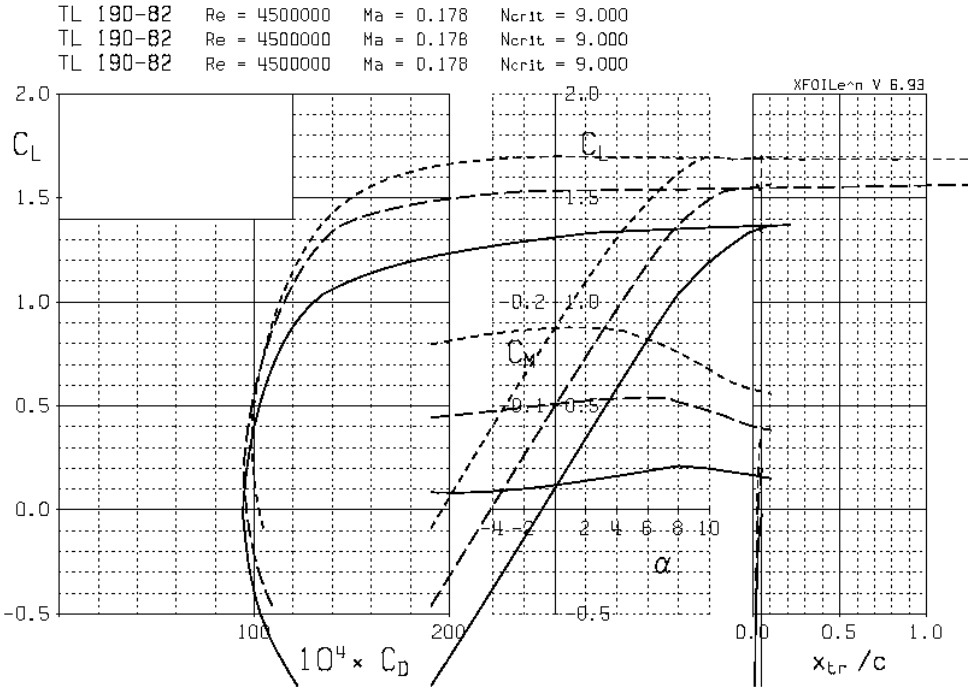

Fig. 5 Predicted polars of the new airfoil for η=-10°/0°/+10° (x_{tr}/c=0.05)

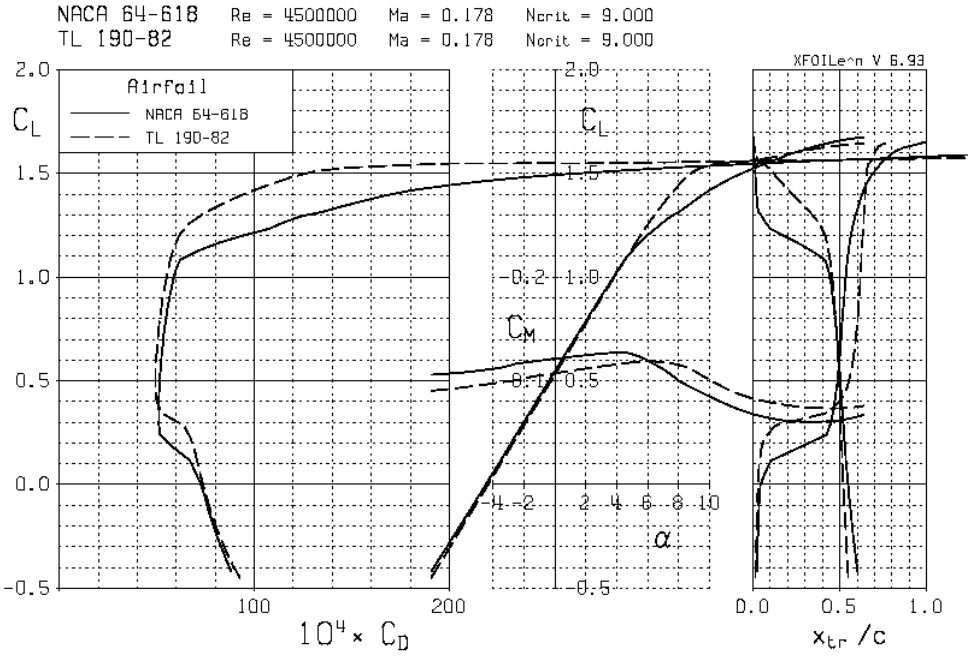

Fig. 6 Predicted polars of the new vs. reference airfoil for η=0° (n=9)

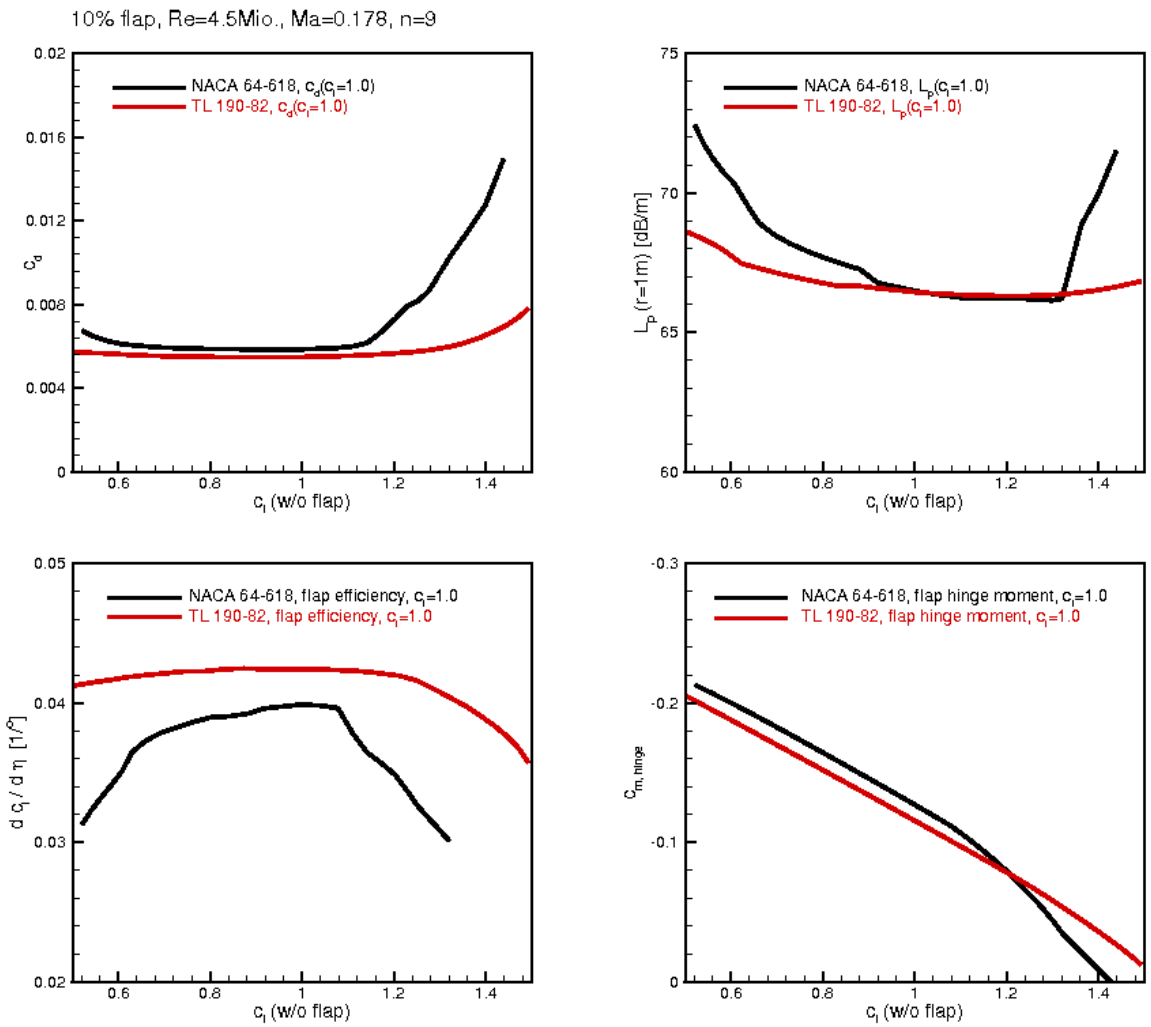

Fig. 7 Aerodynamic and aeroacoustic performance of new vs. reference airfoil

3.4 Unsteady analyses

Besides steady RANS calculations for different flap deflections unsteady analyses have been performed for the NACA 64-618 and the new TL 190-82 airfoils with harmonic oscillating flap. For both airfoils a 10% flap chord was chosen and the deflection amplitude was $\Delta\eta$ = +/- 10°. The calculations were performed for fully turbulent flow and Re = 4.5 · 10^6. The calculations were performed using the CFD solver FLOWer described in Sec. 3.1. The angle-of-attack was chosen such that the lift coefficient amounts to c_l = 1.0 at neutral flap setting. Fig. 8 shows the resulting steady and unsteady lift (left) and moment (right) curves. The steady curves are almost straight but show some bending at high positive flap setting. The depicted unsteady curves were determined for a reduced frequency of the flap motion of k = 0.1. This corresponds roughly to the maximum that occurs at the UPWIND reference turbine with a 3/rev higher harmonic control. The lift curves for the moving flap at this reduced frequency already show typical unsteady characteristics. A hysteresis and a reduced inclination are visible in the lift curves. The unsteady effects seem to be slightly higher for the NACA airfoil. In the moment curves only a slight hysteresis can be observed for the NACA airfoil. The direction, however, is counterclockwise which means that a slight negative aerodynamic damping.

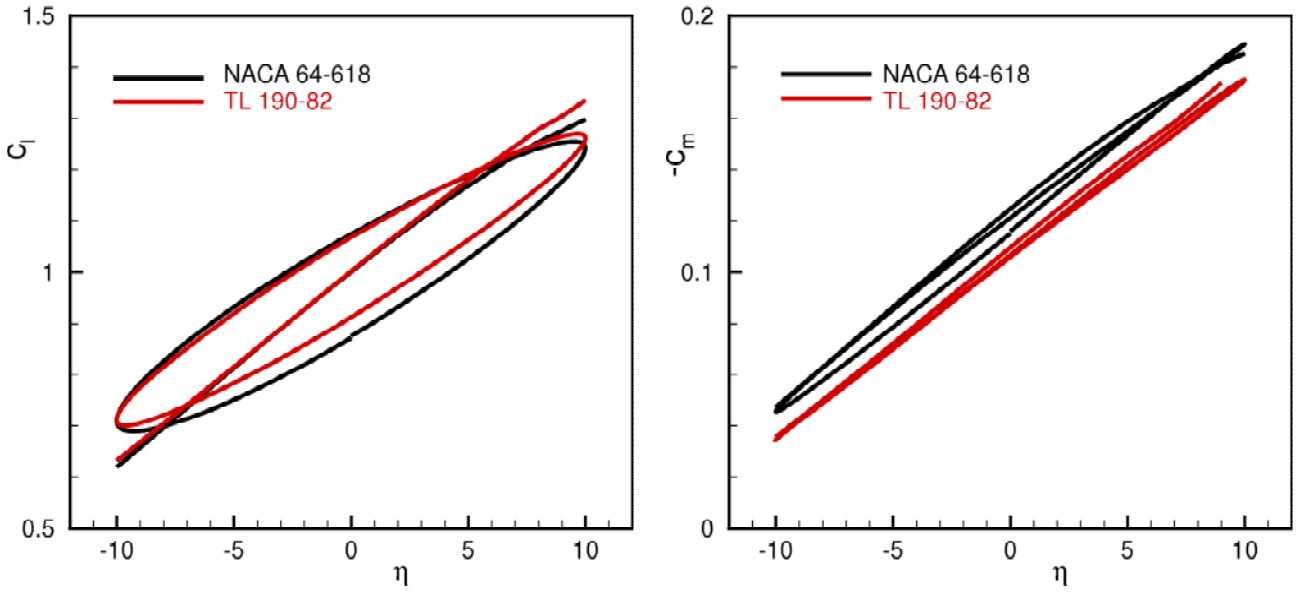

Fig. 8 Unsteady and steady lift curve (left) and moment curve (right) of TL 190-82 vs. NACA 64_3-418 with harmonic flap motion, Re=4.5 · 10^6, fully turbulent, η=+/-10°, k=0.1

4 Steady wind tunnel tests on airfoils with trailing-edge flap

4.1 Wind tunnel and measuring technique

Laminar Wind Tunnel (LWT)

The tests were performed in the Laminar Wind Tunnel (LWT) [Althaus1996] of the IAG, University of Stuttgart. The LWT is an open return tunnel with a closed test section (Fig. 9). The rectangular test section measures $0.73 \times 2.73 m^2$ and is 3.15m long. A 2D airfoil model spans the short distance of the test section and gaps between model and tunnel walls are sealed. The high contraction ratio of 100:1 as well as five screens and filters results in a very low turbulence level of less than $Tu = 2 \times 10^{-4}$ for a frequency range of 20-5000Hz and a flow velocity of 30m/s.

Blowing air tangential in the corners between the model and the mounting plates is used as a boundary layer control to ensure two-dimensional conditions. The nozzles were

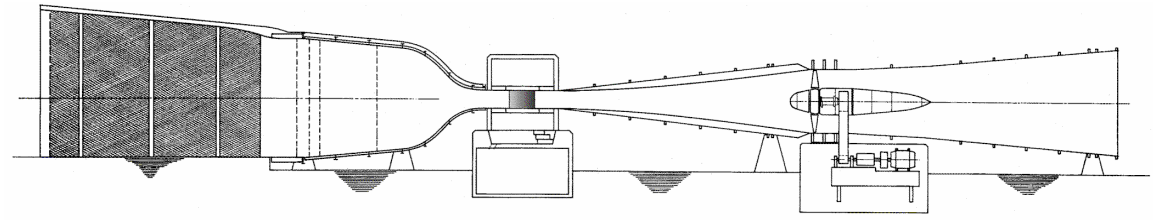

Fig. 9 Sketch of the Laminar Wind Tunnel, total length 46m

placed on the tunnel wall at 0.6 *x/c* of the upper surface of the airfoil, which is the standard position. The influence of the blowing system on the measured lift data is studied in each measuring campaign for a few representative test cases. In general the lift is slightly enhanced, with a stronger effect for positive flap setting. The order of magnitude is in the usually observed range and can be attributed to local corner effects. Therefore, no additional investigations were performed. Nevertheless, it has to be noted that all polar measurements were performed ***with*** corner blowing, whereas the acoustic measurements were performed ***without*** corner blowing. The reason is, that the blowing increases the sound level in the test section.

Polar measurement and wind tunnel corrections

The lift is determined by experimental integration of the pressure distribution along the opposite two tunnel walls. The difference of both averaged pressures is proportional to the lift. In comparison to measurements with a balance it is possible to avoid any gap between model and wind tunnel wall. This is very important especially for high lift systems. The drag is determined by an integrating wake rake, which is positioned approximately 0.45 chord length behind the model trailing edge. The rake automatically travels into the middle of the wake and adjusts itself parallel to the local flow direction. The width of the wake rake is selected according to the expected drag. For the current tests a standard wake rake with a width of 120 mm was used. During measurements the wake rake is traversed in spanwise direction and a mean value for the drag is calculated. For the $NACA64_3$-418 measurements the integration domain of the wake rake was positioned slightly outside the center of the test section to avoid disturbances coming from the pressure taps. To obtain lift and drag coefficients, the undisturbed dynamic head, the static pressure and the maximum pressure loss in the wake are measured as well. The data acquisition system is controlled by a PC and carefully calibrated before each set of measurements.

The reference for the angle of attack is the chord line defined by the coordinates of the airfoil. The reference length for all coefficients is the length c = 600mm of this chord line.

Standard wind tunnel corrections are applied to the coefficients c_l, c_d, c_m and the angle of attack. More information about the wind tunnel corrections is documented in Ref. [Würz2008] and in reports to be downloaded from the Laminar Wind Tunnel homepage [Althaus2003-1], [Althaus2003-2].

Pressure distribution

The wind tunnel model of the NACA airfoil was equipped with pressure taps to measure the pressure distribution. The pitching moment was obtained by integration of the complete pressure distribution (main part and flap). Figure 10 gives an overview of the pressure taps on the NACA 64_3-418 model. The pressure distributions were obtained by a PSI pressure scanning system. A 64 channel pressure scanner with a full-scale range of 350 mbar was used for the measurements at Re = 2.5×10^6 and a similar scanner with 170mbar for the measurements at Re = 1.25×10^6. The transducers were calibrated before every set of measurements against a MKS-Baratron reference pressure transducer. During the measurements the integration time was set to 0.1s per channel, which is sufficient for accurate pressure readings. This time is in fact much shorter than the expected response time of the pneumatic system because of the small diameter of the pressure taps and the long tube connection (≅ 1.5 m) to the transducers. Therefore, the effective time constant with respect to changes in the static surface pressure is in the order of 1 second. This is sufficient for measuring stable flow states (the measurements were done with fixed angle of attack and *not* within an angle of attack sweep). A total of 500 samples were recorded and averaged during the integration time by a 16bit NI-6052E AD-converter card. This provided very stable values in regions of attached flow. In the separated cases a certain scattering is visible, which can only be avoided by very long (several seconds) integration time.

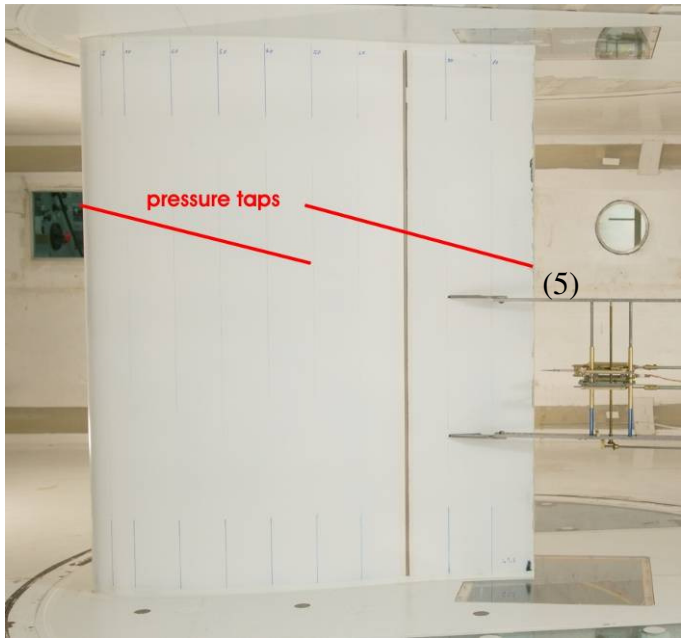

Fig. 10 Location of pressure taps of the NACA 64_3-418 wind tunnel model, view of pressure side

The pressure coefficient c_p is measured according to the following definition:

$$c_{p_i} = 1 - \frac{q_i}{q_\infty} = 1 - \frac{g - p_i}{g - p_\infty}$$

where p_i is the static pressure at every pressure tap, g the total (reference) pressure in the settling chamber of the wind tunnel and p_∞ the static (reference) pressure in the test section.

CPV trailing-edge noise measuring system

The CPV method developed at the Laminar Wind Tunnel was applied for trailing edge noise measurements. Special hot-wires are used for the measurement of particle velocity and the velocity fluctuations are converted to sound pressures assuming sources of monopole type located at the trailing edge. From the phase of the cross correlation function it is possible to distinguish between trailing edge noise and background noise. For details of the method see [Würz2004, [Herrig2005], [Herrig2006]. The hot wires are mounted on two cantilevers which have the shape of a symmetric airfoil, see Fig. 11. The trailing edges of these cantilivers are equiped with serrations to minimize the trailing edge noise emissions of the cantilivers and therefore to minimize the disturbances on the noise measurements of the wind tunnel model. The two cantilivers are mounted on a flat plate which is attached to the turn table and are rotated with the airfoil when α is changed. To guarantee consistent results it must be secured that the wake of the airfoil lies between the both cantilivers. DISA 55M10 hot-wire bridges were used.

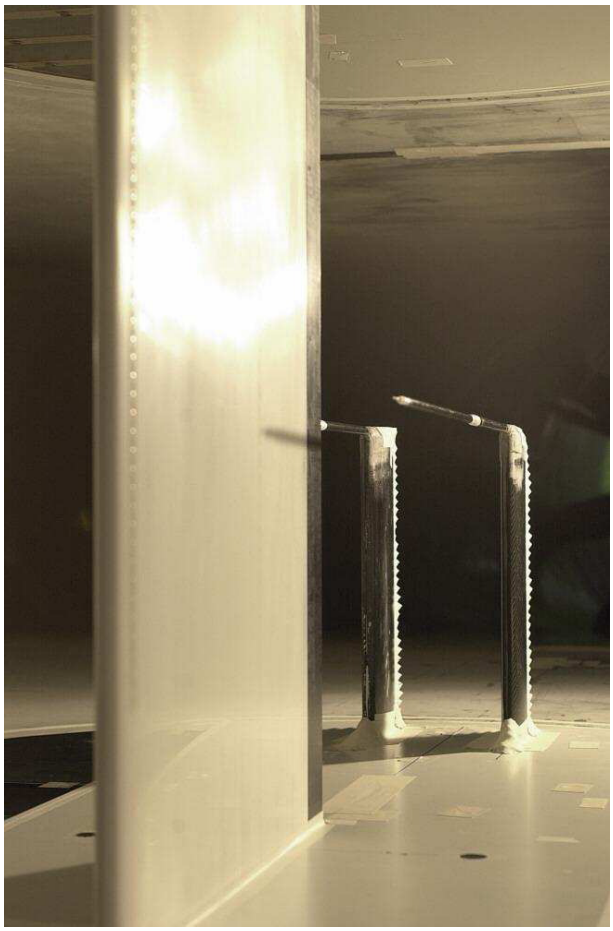

Fig. 11 CPV trailing-edge noise measuring system

Transition detection and turbulators

A thermal camera system was used to check the transition position during the speed-up of the wind tunnel in order to check for the two-dimensionality of the flow. This method takes advantage from the fact that the heat transfer from the surface is different in a laminar boundary layer in comparison to a turbulent one. Therefore, only a small temperature difference (approximately 2° C) between model and free stream is sufficient to provide a picture of the boundary layer state without any disturbances to the flow field.

For both airfoil sections the measurement of the transition position as function of the angle of attack was performed with the help of a stethoscope. A small microphone inside the stethoscope reads the pressure fluctuations in the boundary layer. The signal is amplified and transmitted to an earphone. The turbulent boundary layer can be clearly distinguished from the laminar one by a typical loud broadband noise. In the laminar boundary layer nearly nothing can be heard. The ‘onset’ of transition is characterized by a strong increase in loudness. Comparison to other transition detection methods show that the determined transition ‘position’ is similar to the position where the skin friction starts to increase. Therefore the detected positions are equivalent to those obtained from visualizations with surface oil-film methods.

Several measurements were performed with artificial roughness at the leading edge to

simulate contamination. A 2D tape with a width of 2mm was selected as turbulator to be consistent with previous measurements on wind turbine airfoils. The tape was built up of layers of Chartpack BG6201M tape with a total thickness of $h = 0.36$mm at the lower surface at 0.1 *x/c* and $h = 0.18$mm at the upper surface at 0.05 *x/c*. For the test runs at Re = 1.25×10^6 the height of the tapes was doubled.

4.2 Wind tunnel models

Fig. 12 Negative mold for the NACA wind tunnel model

The wind tunnel models of the NACA 64-418 reference section and the new airfoil TL 190-82 were manufactured at the IAG workshop in CNC-milled negative molds to ensure maximum contour accuracy. A chord length of 0.6m was chosen; the span of the model is 0.73m. The material for the molds is SIKA SLABS M600, polyurethane foam with a very high density. A special milling technique with an inclined face cutter provides a surface roughness smaller than +0.02mm. This roughness is smoothed by carefully sanding until all milling tracks disappear (Fig. 12 shows the negative molds). Then epoxy resin is used to remove the porosity of the surface. The shells of the models were built as a symmetrical carbon-fiber/glass-fiber/carbon-fiber sandwich with 6 mm wall thickness. After finishing the remaining roughness heights of the wind tunnel models are in the order of 1.5 µm RMS measured with a high precision surface measuring instrument. For acoustic measurements the trailing edge thickness is an important parameter. It must be kept very thin to avoid blunt trailing edge noise which would otherwise spoil the measurements. The design coordinates of the airfoils were modified by rotation of the upper surface around the leading edge to provide thin trailing edges of 0.3 mm thickness. During the whole manufacturing process great care is taken to achieve a trailing edge thickness as close as possible to the nominal value.

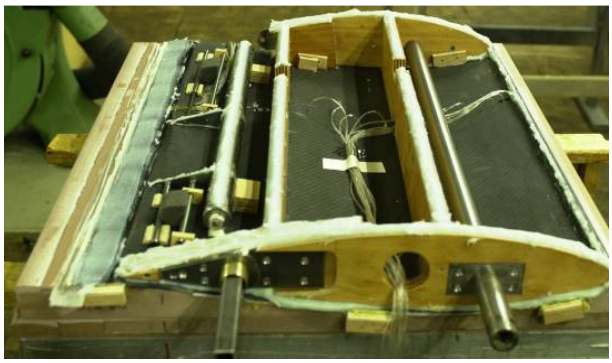

Fig. 12 Complete internal structure of the NACA 64-418 model before glueing

The NACA wind tunnel model was equipped with a row of pressure tabs along the upper and the lower side. Each row is aligned at an 15° angle relative to the freestream. The holes have a diameter of 0.3mm and were drilled making use of a NC-milled template to ensure the correct position and angle of the holes. Fig. 12 shows the complex internal structure of the NACA wind tunnel model.

A flap of 30% was chosen for the NACA model to enable a broad variation of the pressure recovery which was required for complementary fundamental boundary-layer and acoustic measurements performed in UPWIND WP2.5 to improve and validate the noise prediction models developed at the IAG. The pivot point is located midway between upper and lower

side contour. The flap was cutted from the main part of the wind tunnel model. The nose of the flap was built from SIKA SLABS M600 as a positive part. This peace is exactly circular around the flap hinge and fits tangential to the surface contour on the upper and lower side of the model. The gap between flap and main part has a width of 1mm and allows flap deflections of $\beta = \pm 20°$. An internal sealing made of V-seal tapes provides air tightness of the flap. Fig. 13 gives an overview of the flap mounting.

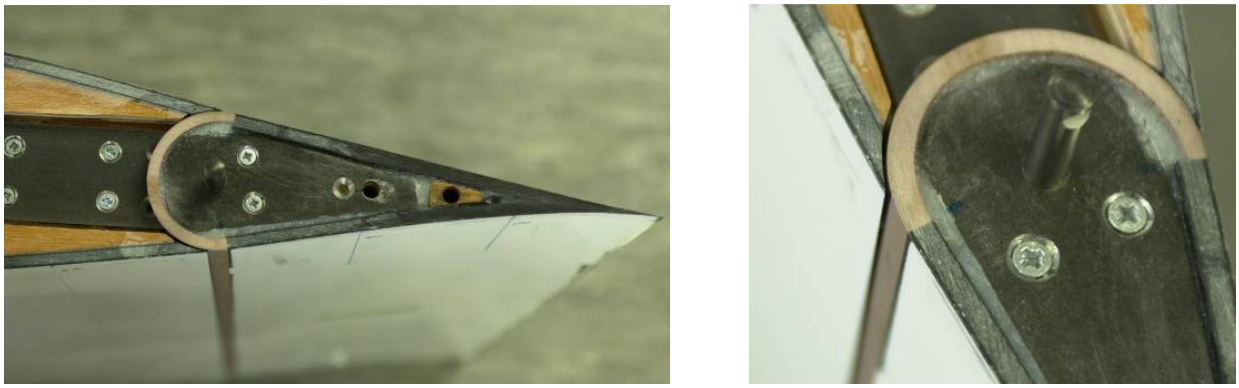

Fig. 13 Details of the flap conjunction

The wind tunnel model of the new airfoil has a chord length of 0.6m and was built in the same way as described above but without pressure taps. In contrast to the reference section the wind tunnel model of the new airfoil shows a smaller chord of only 10% chord that is considered sufficient for load alleviation purposes. The gap between flap and main part has a width of 1mm and allows flap deflections of β=+/-20°. Fig. 14 shows the negative mold and a side view of the wind tunnel model.

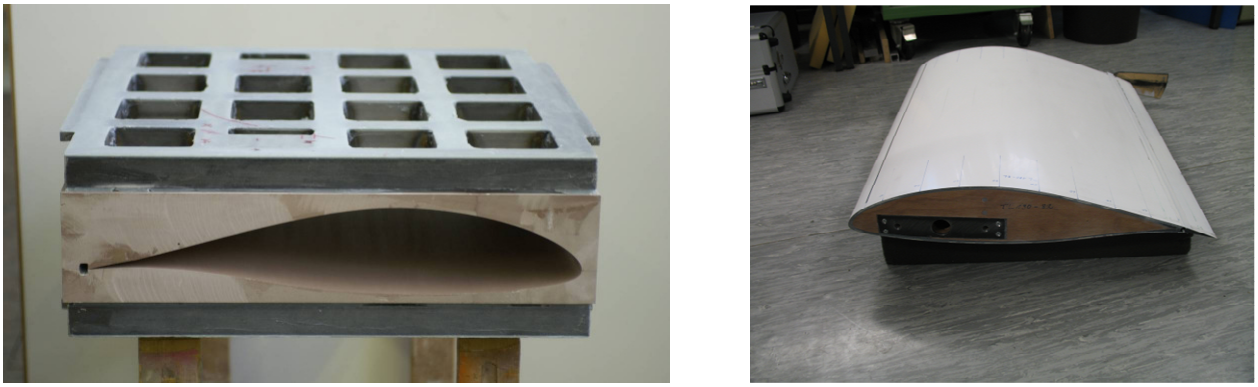

Fig. 14 Negative mold and side view of the TL 190-82 wind tunnel model

4.3 Exemplary results of the NACA 64_3-418 measurements

Polar measurements

The standard procedure for polar measurements was applied. With this procedure the evaluation of lift and drag starting with the lowest angle of attack. The angle of attack is increased until c_{lmax} is exceeded. Then the angle of attack is reduced and additional points were collected if a hysteresis of the c_l-α curve is visible. Hysteresis effects are always carefully checked. The same procedure was done in a similar way for the negative part of the c_l-α slope. Drag measurements were performed, if possible. For all polar

measurements the blowing system was switched on.

Figs. 15 and 16 show the measured polars of the NACA reference airfoil at Re=2.5 · 10^6 for five different flap deflections, namely η=0° / 2.5° / 5° / 7.5° / 10°. Whilst Fig. 15 gives the results for natural transition, Fig. 16 represents the 'rough' case with a turbulator being applied at 5% chord on upper and lower side.

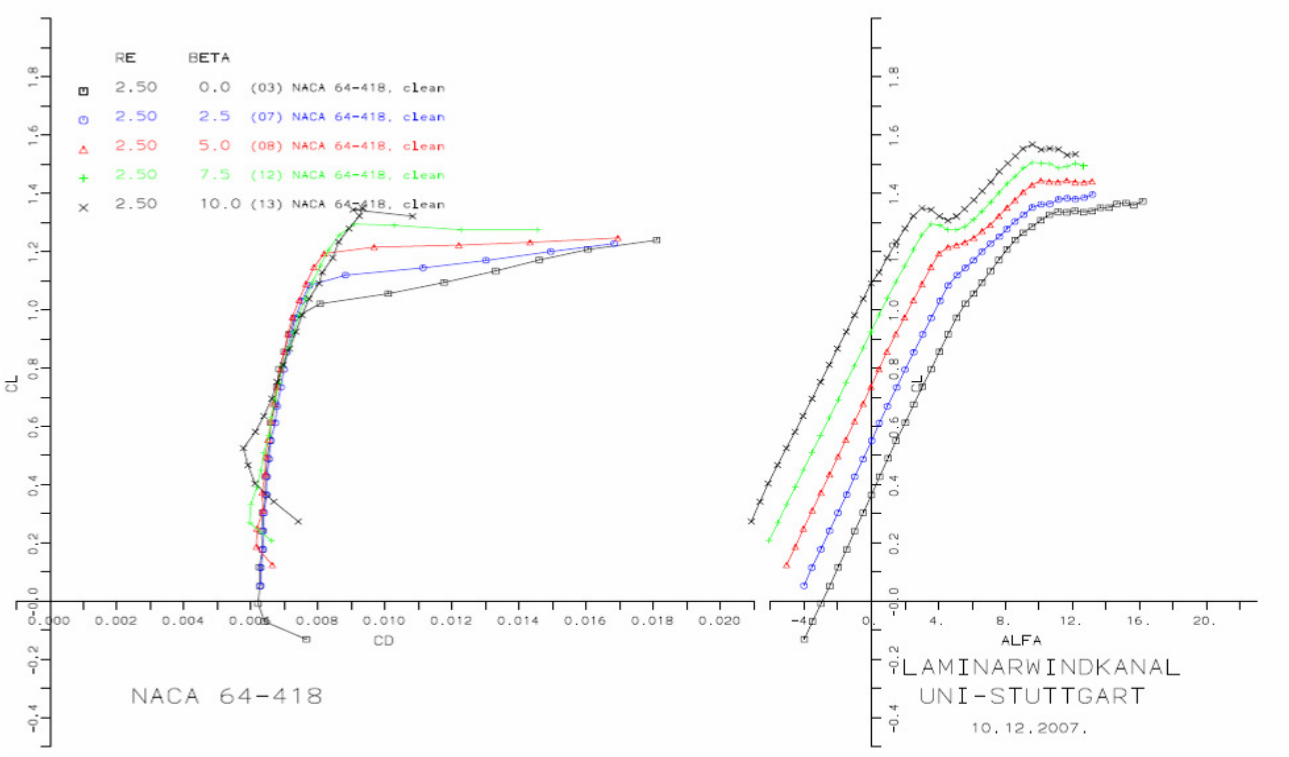

Fig. 15 Measured polars NACA 64_3-418 with 30% flap, Re=2.5×10^6, 'clean' case

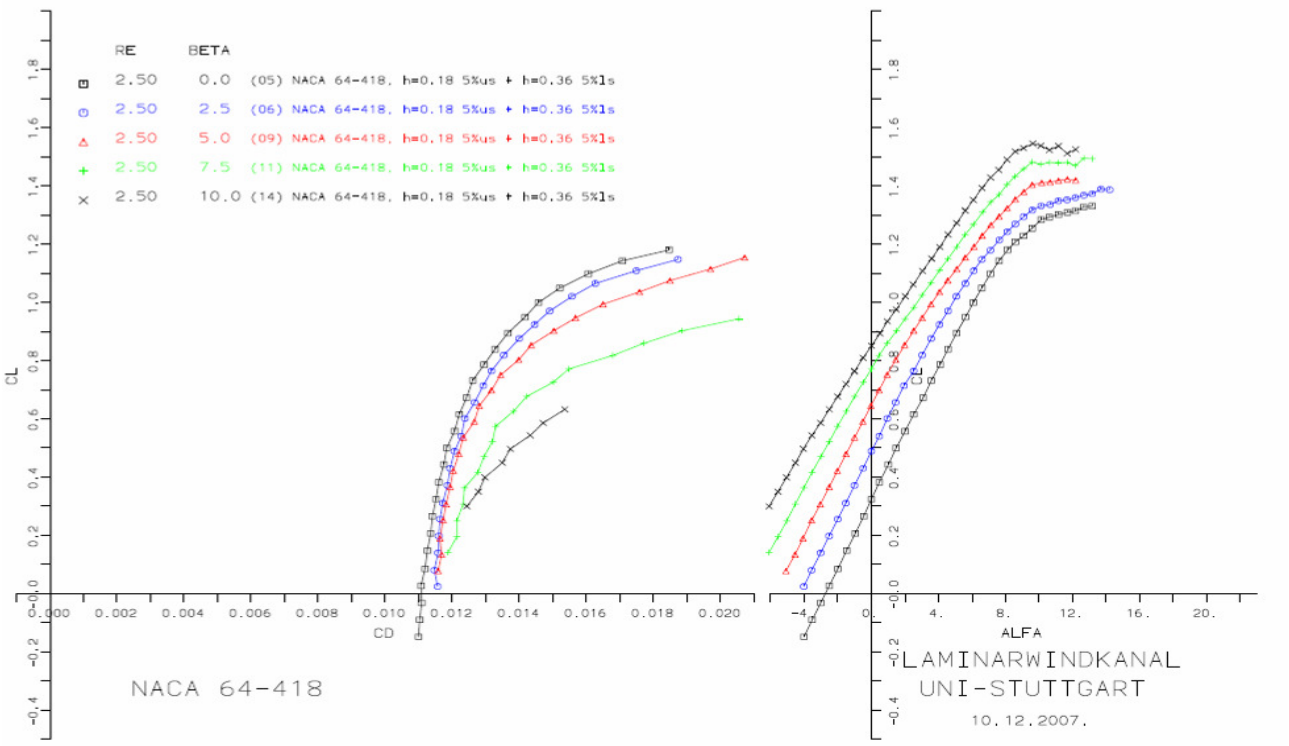

Fig. 16 Measured polars NACA 64_3-418 with 30% flap, Re=2.5×10^6, 'rough' case (tripped at 5% upper and lower side)

Transition detection and flow visualizations

The transition location has been determined by the use of a stethoscope (Sec. 4.?) for different flap settings, flow conditions and angle of attack with the results being documented in Ref. [Würz2008]. Additionally flow visualizations were performed to check for turbulent separation. The separation measurements were performed in particular to examine the impact of a traversing system downstream of the trailing edge used for detailed turbulence and correlation measurements in UPWIND WP2.5. It should be mentioned that this traversing system was not present in the aerodynamic and acoustic measurements documented in Sec. 4.4. Selected results of the flow visualization for neutral flap position are depicted in Fig. 17 (natural transition) and Fig. 18 (tripped case).

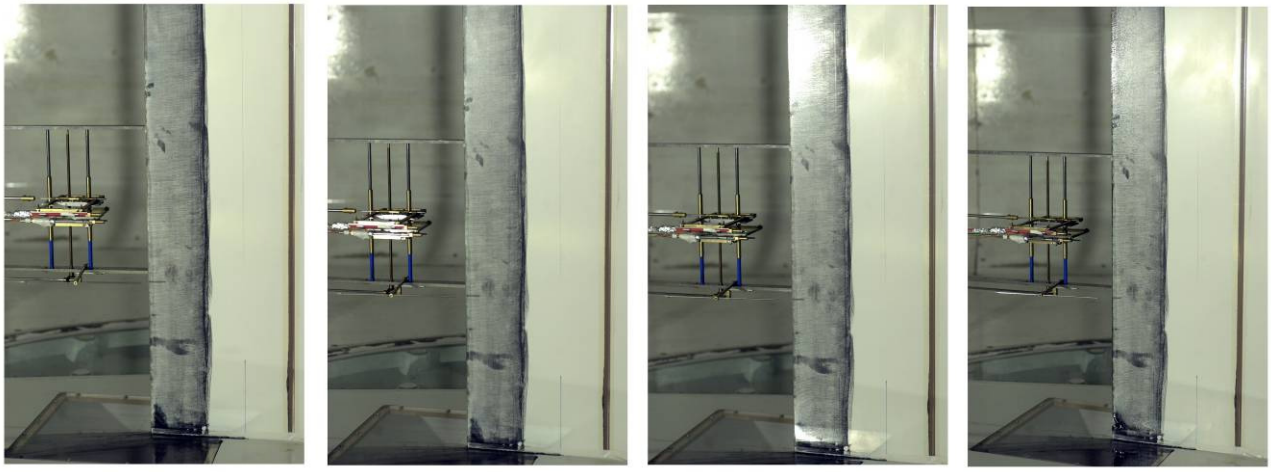

Fig. 17 Re = 2.5×10^6, $\beta = 0°$, 'clean', with traverse, α = -3/0/3/6, corner blowing on

Results for further flow conditions are reported in Ref. [Würz2008].
Fig. 18 shows that the traversing mechanism had a non-negligible influence on the turbulent boundary layer separation at high angle of attack and tripped conditions. For $\alpha = 6°$ the separation is shifted forward by approx. $\Delta x = 0.08$ in the vicinity of the traversing system. For the clean case (Fig. 17) there is no earlier separation due to the traversing system visible.

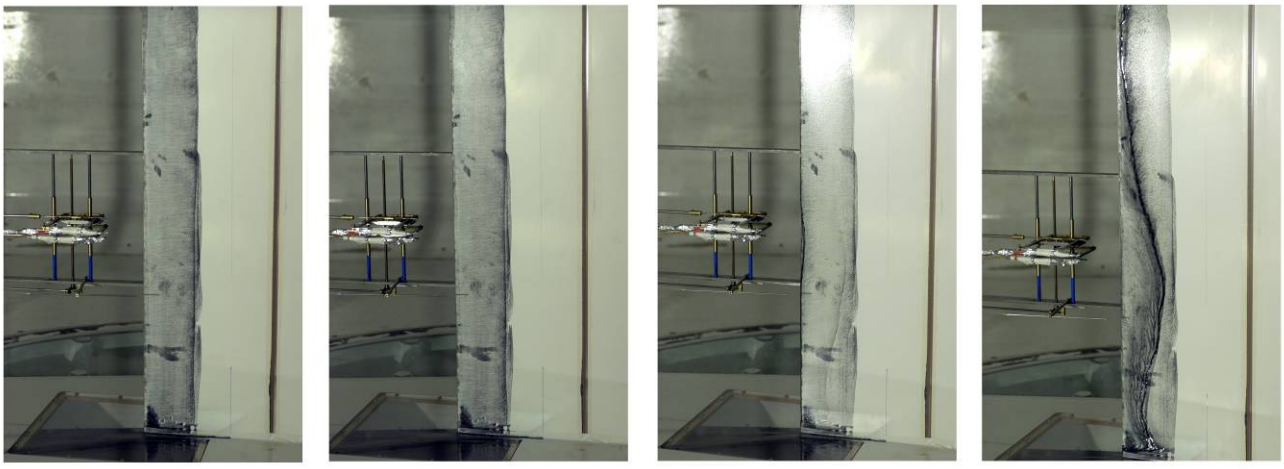

Fig. 18 Re = 2.5×10^6, $\beta = 0°$, 'rough', with traverse, α = -3/0/3/6, corner blowing on

Pressure distributions

The c_p-distributions were measured simultaneously with the normal polar measurements. Therefore, for every polar measurement point a pressure distribution is obtained. From those single pressure distributions polar data were evaluated. No wind tunnel corrections were applied to the measured c_p-distributions.

Examples of the measured c_p-distributions for the 'clean' case are shown in figure 19.

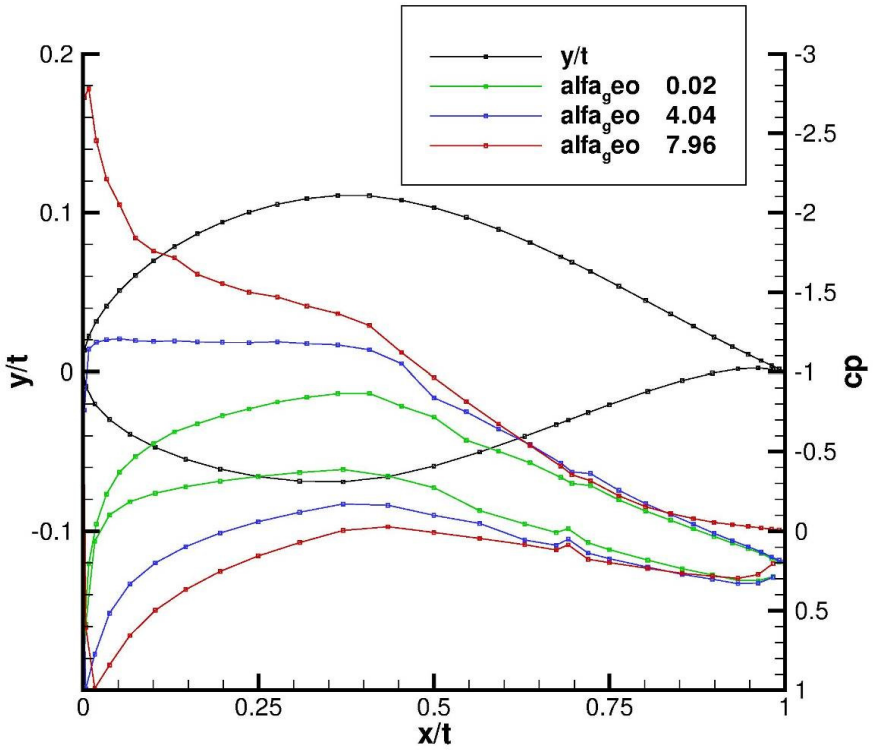

Fig. 19 NACA 643-418, Re=2.5×106, β = 0°, 'clean'

The pressure distributions are quite smooth, showing the high quality of the airfoil model. A small irregularity is visible for x/c = 0.7 as a result of the flap conjunction.

Trailing-edge noise and boundary-layer profiles

Instead of a constant Reynolds number a constant free stream velocity of 70 m/s was selected for the CPV trailng-edge noise measurments. In the figures 20 and 21 exemplary results of CPV and boundary-layer measurements for zero flap deflection are shown while report [Wolf2009] gives more results for other flap settings. In each figure the mean velocity profile of the suction side, the velocity fluctuations in wall normal direction, the integral length scale Λ_2 and the noise spectra are shown. It must be mentioned that the shown turbulence parameters were measured in another test campaign where a velocity of 62m/s was used instead of 70m/s. Looking first on the results for the untripped case with a flap deflection of η=0° (Fig. 20) it can be recognized that with increasing angle of attack the maximum of the noise spectrum moves to lower frequencies and the peak value increases. At high frequencies the noise is reduced for increasing angle of attack α. This behaviour corresponds well with the results for the velocity fluctuations. The maximum is shifted away from the wall with increasing α. The maximum value is also increased. Looking at the Λ_2 results it can be easily seen that they increase with increasing angle of attack. This corresponds well with behaviour of the discussed velocity fluctuation results.

Comparing these results with the tripped case shown in Fig. 21 it can be said that the general behaviour is the same like for the clean case. The noise spectra, however, are shifted to higher levels as the boundary-layer is thicker and shows stronger fluctuations near the trailing edge compared to the clean case. This is confirmed by the measured velocity fluctuations and Λ_2 values, which are increased, too.

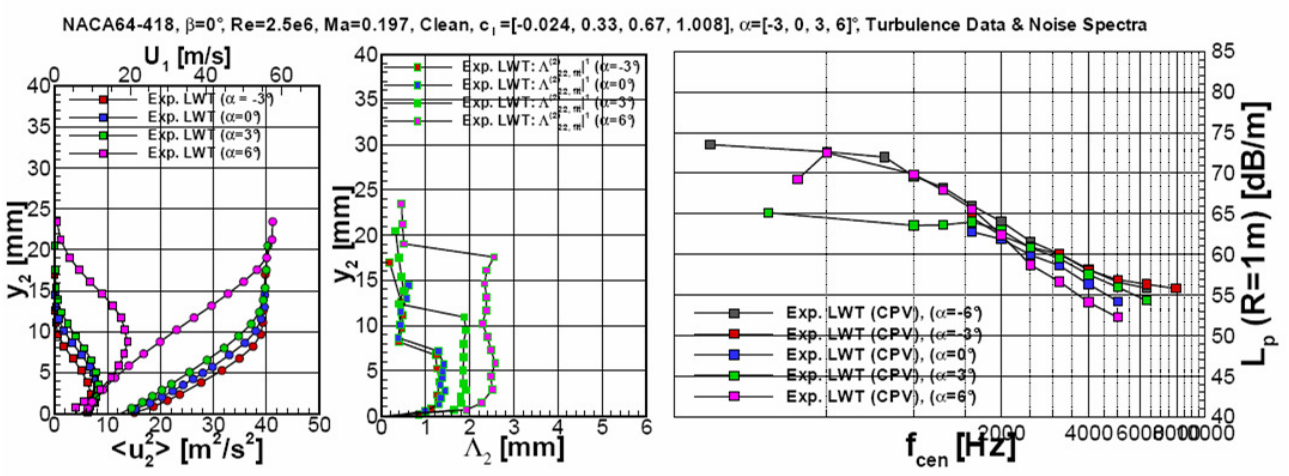

Fig. 20 Measured boundary layer profiles and trailing-edge noise spectra NACA 64_3-418, η=0°, Re=2.5×10^6, 'clean' case

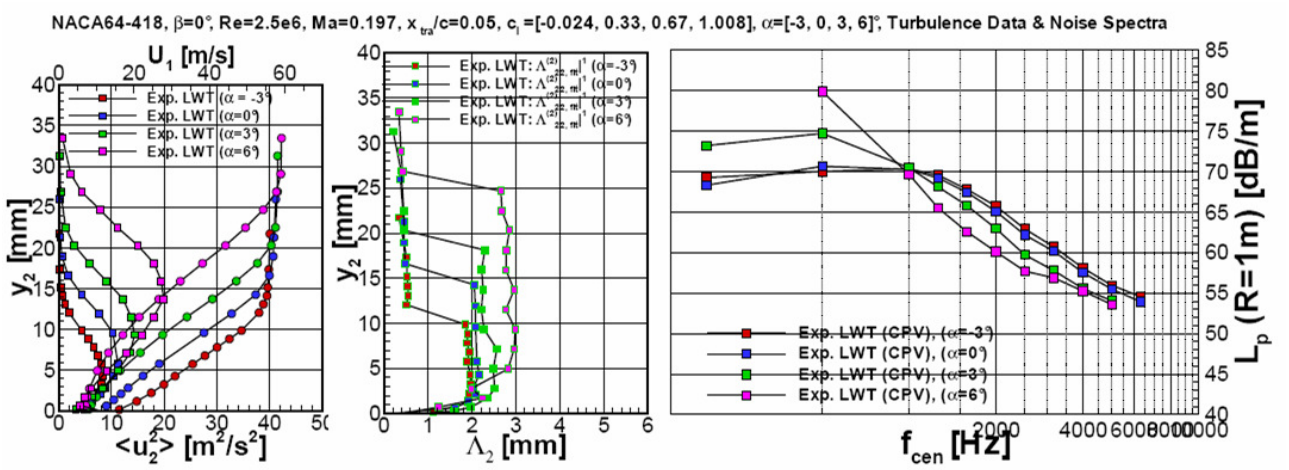

Fig. 21 Measured boundary layer profiles and trailing-edge noise spectra NACA 64_3-418, η=0°, Re=2.5×10^6, 'rough' case

4.4 Exemplary results for the new airfoil TL 190-82

Detailed aerodynamic and aeroacoustic measurements were performed for the new airfoil TL 190-82. The experiments include polar measurements and localization of transition and separation locations as well as CPV trailing-edge noise measurements for different flap settings. The measurements are documented in Ref. [Wolf2010]. Below, exemplary results are presented.

Polar measurements

The same procedure as described in Sec. 4.3 was applied in the polar measurements of the new airfoil TL 190-82 with a 10% flap chord. For all polar measurements the blowing system was switched on. Figs. 22 and 23 show the measured polars at Re = $2.5 \cdot 10^6$ for

five different flap deflections, namely η=0° / 2.5° / 5° / 7.5° / 10°. Whilst Fig. 22 gives the results for natural transition, Fig. 23 represents the 'rough' case with a turbulator being applied at 5% chord on upper and lower side. Additionally polars were measured for Re = $1.5 \cdot 10^6$ and Re = $3.3 \cdot 10^6$ [Wolf2010].

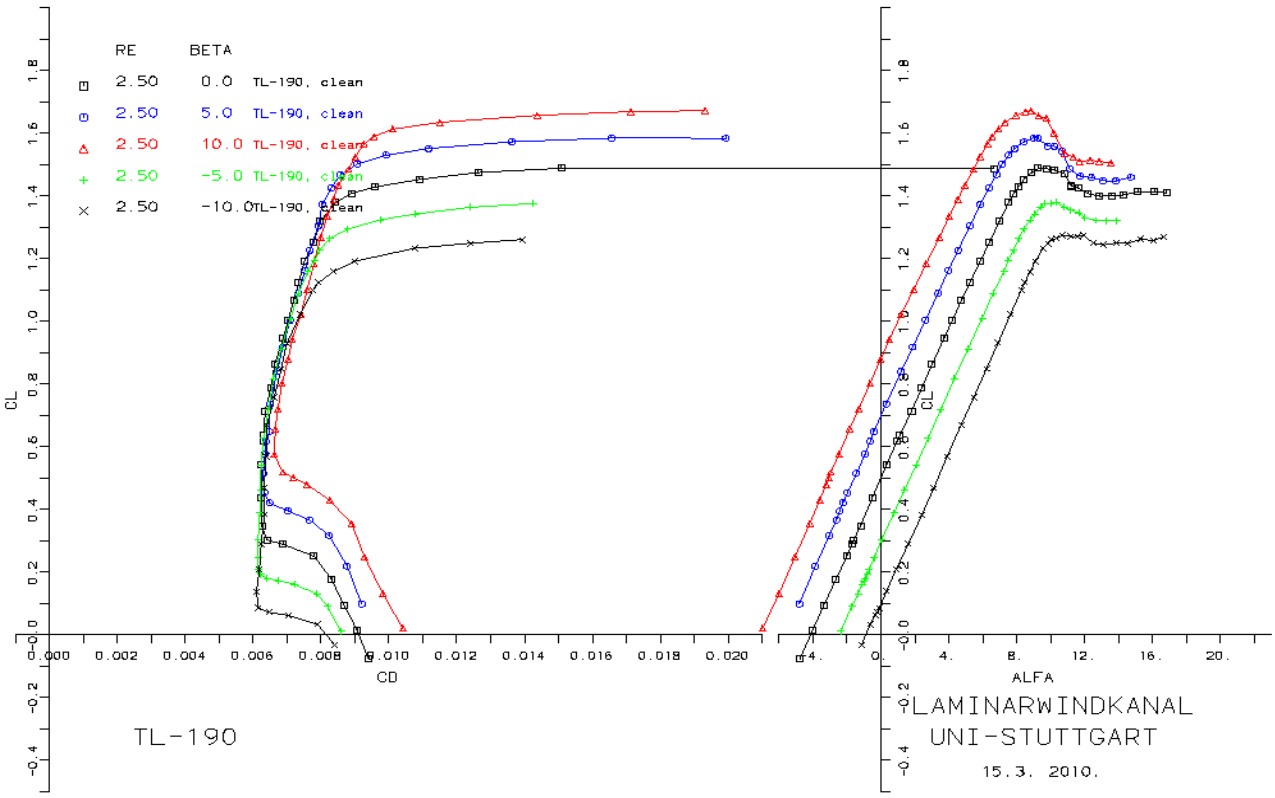

Fig. 22 Measured polars TL 190-82 with 10% flap, Re=2.5×10^6, 'clean' case

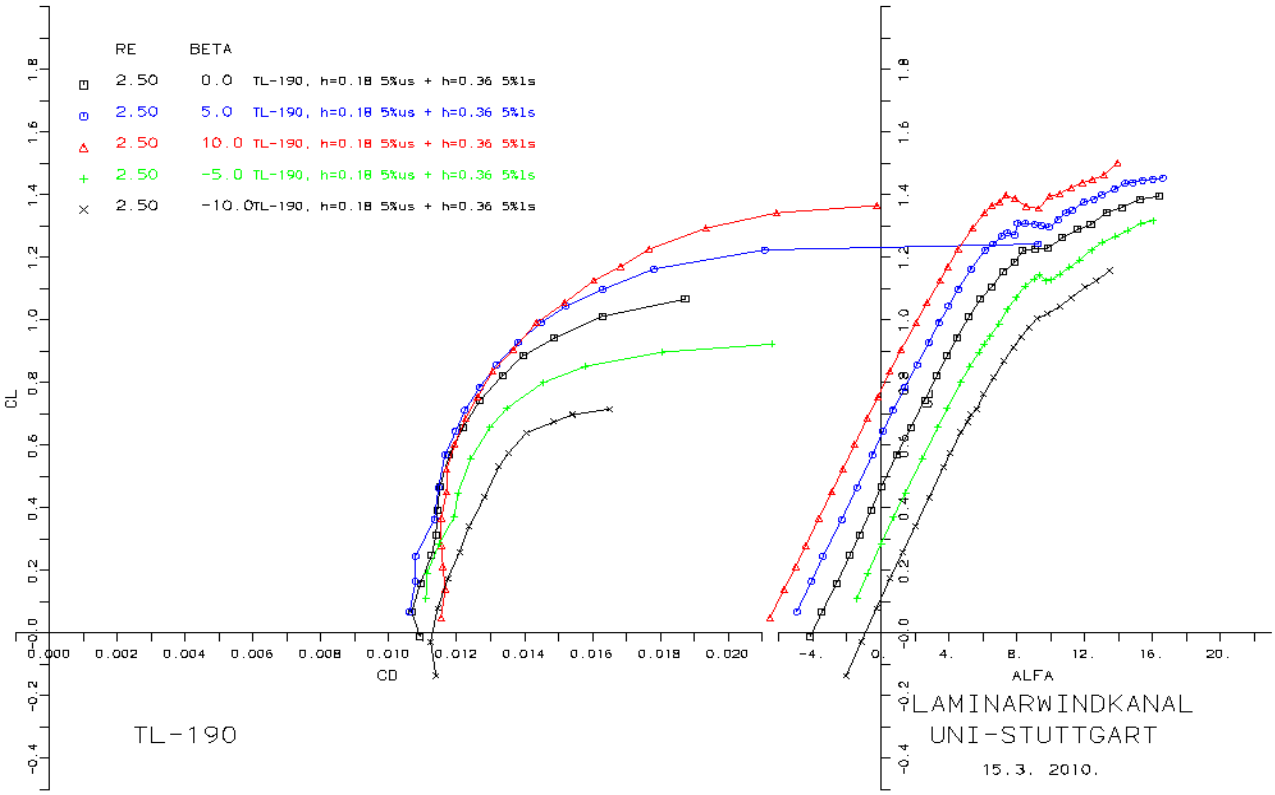

Fig. 23 Measured polars TL 190-82 with 10% flap, Re=2.5×10^6, 'rough' case

Trailing-Edge Noise Measurements

CPV trailing-edge noise measurements were performed for different flap settings at constant lift coefficients of c_l = 1 and c_l = 0.7 respectively. The corresponding angles-of-attack were determined in advance for flap settings of η = -10° / -7.5° / -5° / -2.5° / 0° / 2.5° / 5° / 7.5° / 10°. To minimize the level of the background noise the blowing system was switched off during the AoA determination and the CPV measurements. In case of c_l = 1 no measurements for the tripped case with negative flap deflection were performed, as separation occurred for the low Re of the present experiments. The disturbance caused by the separation lead to a shaking of the CPV-system. This causes uncertainties in the acoustic measurement and increases the risk of structural collapses of the CPV system.

Instead of a constant Reynolds-number a constant free stream velocity of 70 m/s was chosen for the CPV measurements. Figure 24 shows the results of the clean cases at c_l = 0.7 and 1.0. A noise reduction can be recognized for a positive deflection, while for negative flap setting the noise is increased compared to the baseline with no flap deflection. An impact of the flap deflection on the noise level can be mainly observed at high and low frequencies respectively. This general behaviour is the same for both c_l values. But for a c_l of 1 the noise increase and reduction by flap deflection are even higher.

The tripped cases show generally the same trend like the clean cases (see Figure 25). For c_l = 1 the impact of the flap deflection on the noise level is much higher than for the other cases. But the trend is nearly the same. For negative flap deflections a massive noise increase can be seen at lower frequencies.

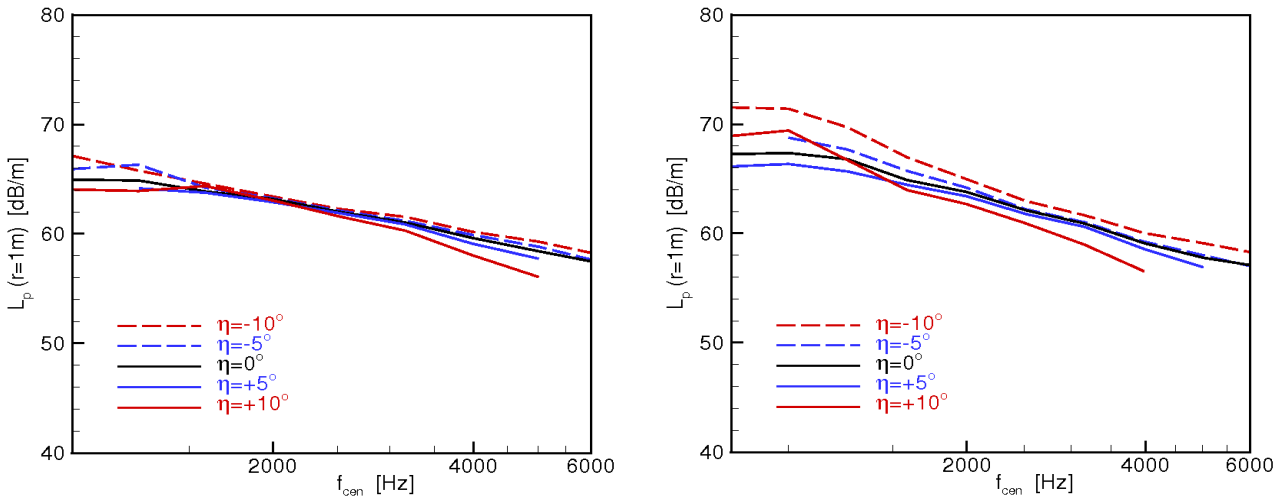

Fig. 24 Measured noise spectra TL 190-82 with 10% flap, Re=2.5×10^6, 'clean' case (left: c_l = 0.7, right: c_l = 1.0)

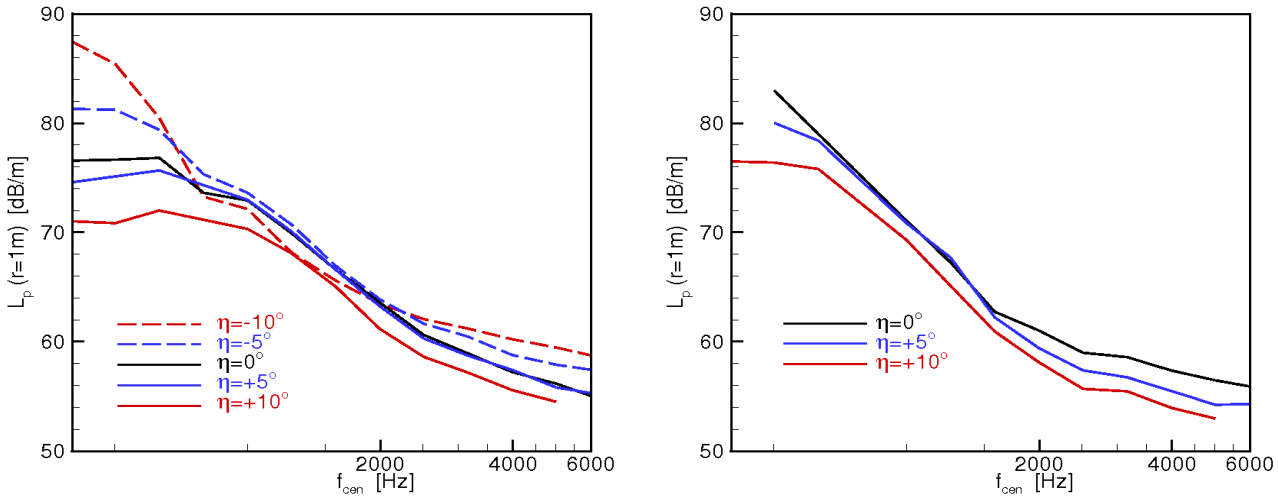

Fig. 25 Measured noise spectra TL 190-82 with 10% flap, Re=2.5×10^6, 'rough' case case (left: c_l = 0.7, right: c_l = 1.0)

4.5 Comparison of the airfoils

Subsequently some selected experimental results for the new airfoil shall be compared to the results obtained for the NACA 64_3-418 section in order to supplement the numerical assessment of the new design as discussed in Sec. 3.3. Figs. 26 and 27 show the measured and XFOIL predicted polars for natural transition and tripped conditions respectively. The clean configuration without flap deflection is considered. From Fig. 26 it is obvious that the laminar bucket of the new airfoil is shifted to significantly higher c_l-values. This can partly be attributed to the fact that the present NACA 64_3-418 reference has a smaller camber than the NACA 64-618 airfoil actually applied in the UPWIND turbine. Another reason is that, according to the design objectives described in Sec. 2.3, the new airfoil was designed to show small drag at c_l=1.0 also for negative flap deflection. This necessitates the extension of the laminar bucket to higher values. Even though the camber and thus the over-velocities on the suction side are higher for the new airfoil a drag reduction could be achieved compared to the NACA airfoil. This is a result of an optimized pressure distribution to delay transition and reduce turbulent skin friction in the pressure recovery region. The XFOIL calculations in combination with the full e^n transition prediction agree quite well with the measured drag polars although the predicted drag level is slightly smaller. This is a general tendency also observed for other comparisons of XFOIL with wind tunnel results.

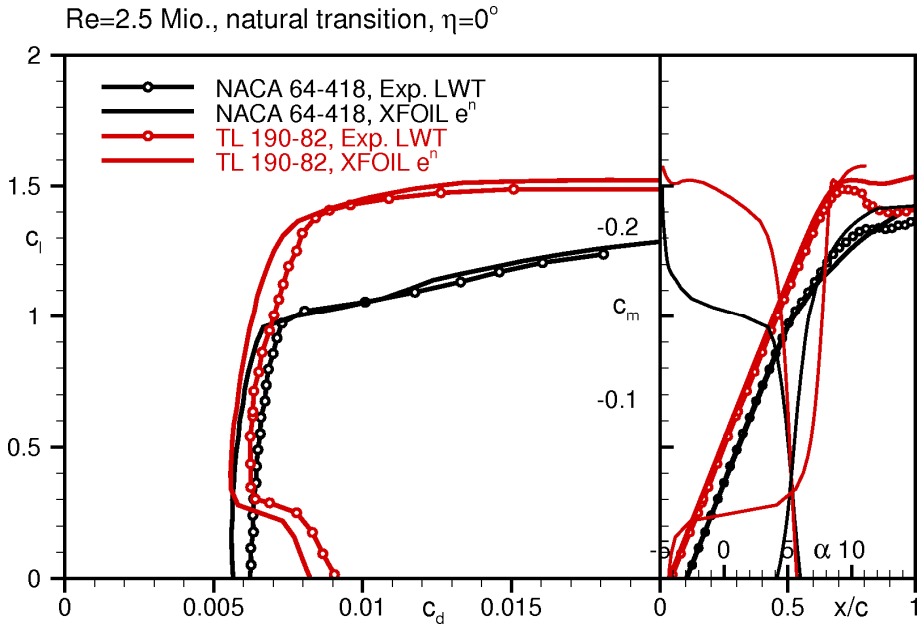

Fig. 26 Measured and predicted polars TL 190-82 vs. NACA 64_3-418, Re=2.5×10^6, η=0°, 'clean' case

Fig. 27 depicts the results for tripped boundary layer. Again, XFOIL is too optimistic, i.e. the predicted drag level is lower than the measured results. Also the maximum lift coefficient is over-predicted. For the rough case the performance of the new section shows no improvement compared to the NACA section, at higher c_l the drag is even slightly higher. This is mainly caused by the considerably higher camber and the associated high over-velocities and stronger pressure recovery on the suction side. The behaviour can also be attributed to the low test Reynolds number (Re = 2.5 · 10^6) which is well below the main design Reynolds number (Re = 4.5 ·10^6).

Fig. 28 finally shows the impact of a flap deflection on the polars for natural transition. It is obvious that the drag polars of the new airfoil are shifted almost parallel in c_l direction by the flap deflection, no negative impact on the drag is visible outside of the laminar bucket. The flap efficiency seems to be high considering the fact that the flap chord of the new airfoil amounts to only 10% while the flap of the NACA model was 30% chord. The drag level of the envelope of the polars is smaller for the new airfoil within the whole c_l regime.

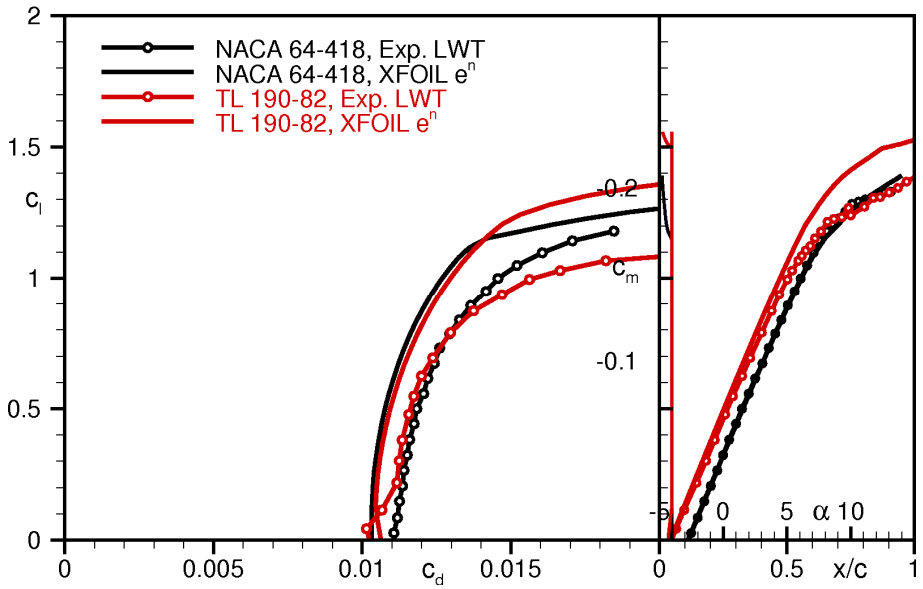

Fig. 27 Measured and predicted polars TL 190-82 vs. NACA 64_3-418, Re=2.5×10^6, η=0°, 'rough' case

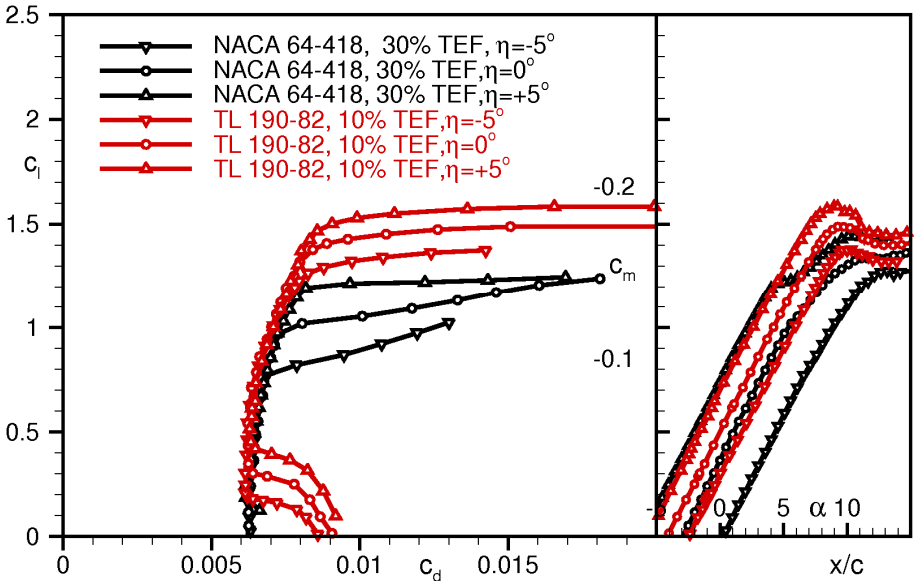

Fig. 28 Measured polars TL 190-82 (10% flap) vs. NACA 64_3-418 (30% flap) for different flap settings, Re=2.5×10^6, η=0°, 'clean' case

5 Unsteady wind tunnel tests on an airfoil with flap and mini-flap

Main objectives

LM wind Power contribution to the project is to design and test two aerodynamic solutions for unsteady distributed load control on wind turbine blade. After a non-exhaustive survey the two most promising concept to be tested in LM wind tunnel are the flap and the mini-flap.

Wind Tunnel setup

The LM Wind Power wind tunnel has an airline with a closed return loop (Figure 29). The overall outside dimensions are 37 m x 14 m. The airline layout is traditional with diffusers between corners, a single stage fan, a settling chamber and a contraction. The diffusers as well as the corners are rectangular, except for the in- and out-lets of the fan. The diffusers expand only in the vertical direction between corners, whereas the corners expand in the horizontal direction. The use of expanding corners is an innovative feature that reduces the overall loss in the airline as well as the overall size of the airline. Also, this avoids the need of a wide angle diffuser in front of the settling chamber. To make this feasible, the corners have tailored vanes with optimized cascade airfoil shapes. The fan has a maximum power consumption of 1 MW which is sufficient to maintain a flow velocity of 105 m/s in the test section with an inclined airfoil with a chord of 900 mm. The cooling system is dimensioned to keep temperature constant at all fan powers. A honeycomb structure is straightening the flow and three subsequent turbulence screens are dampening out fluctuations. The contraction has a ratio of 10:1.

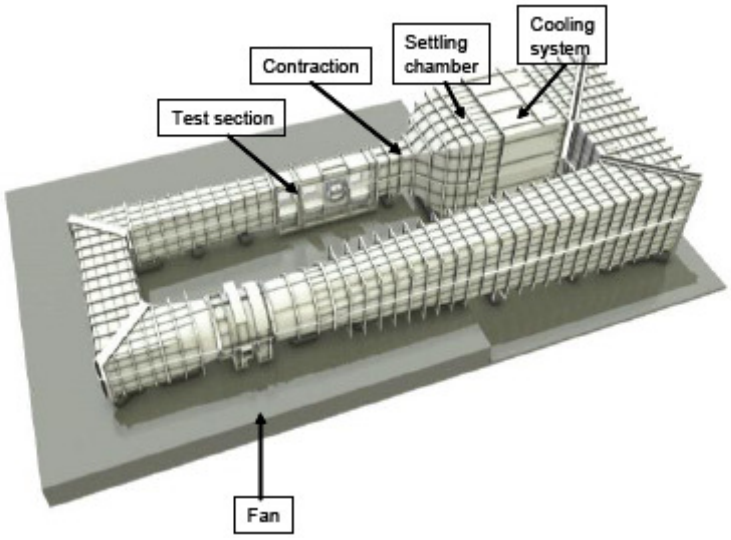

Fig. 29 View of LM Wind Power wind tunnel airline

The main purpose of the facility is to do 2D aerodynamic testing of wind turbine airfoils, as shown in 30. The test section contains the airfoil model between the two turn tables and the angle of attack (AoA) of the airfoil model relative to the horizontal inflow is changed by turning the turn tables. A horizontal and vertical traverse is installed downstream of the turn tables with a horizontal beam in the test section with a probe holder that moves in the horizontal direction. This holds a wake rake, which is a structure with a row of total and static pressure tubes to measure the deficit from the airfoil wake. The primary angle of attack range for the airfoil is from -20° to 30° to cover the normal operation range of a rotor blade, which is within the negative stall angle and the angle of attack where leading edge stall occurs.

Regarding the flow quality of the test section, the longitudinal component of the turbulence

intensity was 0.1 for a flow speed of 100 m/s (high pass filtered at 10 Hz). The variation of the flow in both time and space was found to be less than 0.2% of the free flow velocity and the angularity was less than 0.2^{o}.

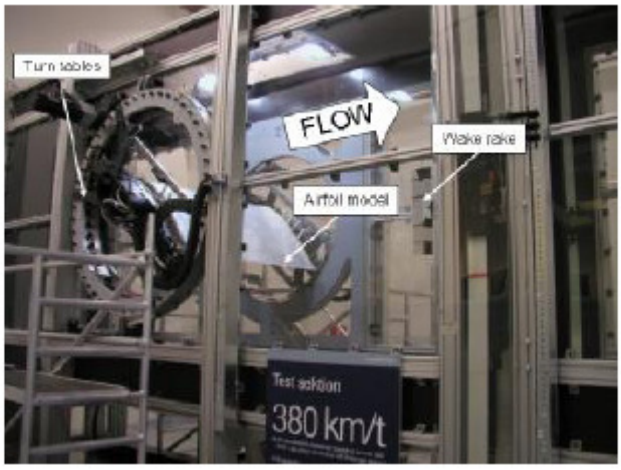

Fig. 30 Side view of test section with an airfoil model between the two turn tables

A total of 276 signals are measured. These are mainly differential pressures in addition to a six component load balance system on the turn tables and measurements of various test section flow properties.

Fig. 11 shows an overview of the measured signals:

- The airfoil model is equipped with pressure tabs on the upper and lower surfaces in the centre region to measure the pressure distribution.
- The test section floor and ceilings are equipped with pressure tabs to measure the static pressure variation in longitudinal and transverse directions.
- The wake rake downstream of the airfoil is equipped with total and static pressure tubes to measure the vertical pressure distributions.
- The load balance system on the turn tables measure airfoil model forces.
- The inflow angle of attack is measured directly from the turn table encoder positions, knowing the alignment of the airfoil model.
- Additional test section flow properties include temperature, free stream flow velocity /dynamic pressure and atmospheric pressure.

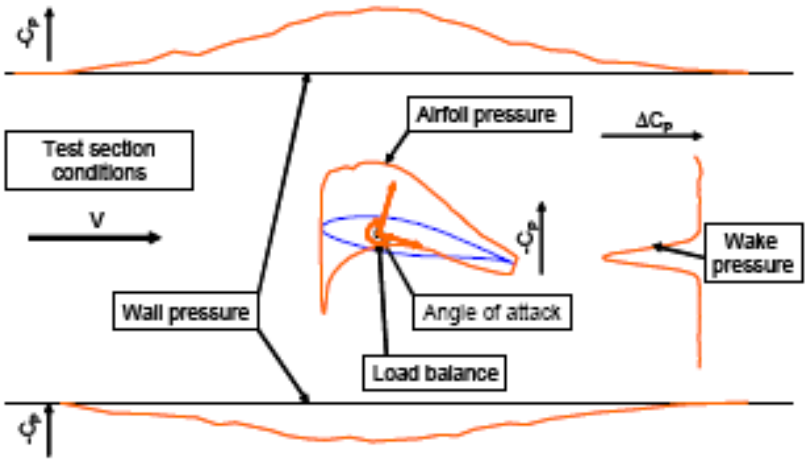

Fig. 11 Overview of measurement signals in the test section

The measured pressure distributions and the load balance signals can be used to derive the airfoil force coefficients:

- The airfoil pressure distribution is used to calculate the lift and moment coefficients as well as the pressure drag coefficient, which is typically used as a good approximation to total drag at separated flow.
- The floor and ceiling longitudinal pressure distributions are used to calculate the lift coefficient, which is only valid for attached flow at angles of attack below the maximum lift coefficient.
- The wake rake total and static pressure distributions are used to calculate the total drag coefficient, which is valid only when the airfoil flow is attached.
- The load balances on the turn tables are used to calculate airfoil lift, drag and moment coefficients.

Wall corrections are applied to derive correct results.

Airfoil model setup

LM Wind Power has decided to test two unsteady devices the flap and the mini-flap. The main difference between the two systems is the size of the active part of the airfoil. The flap is 10% chord length when the mini-flap is only 1%. The airfoil tested has a maximum thickness of 24%. It has been design internally in LM for wind turbine purpose and is widely used on the newest LM blades around mid span position.

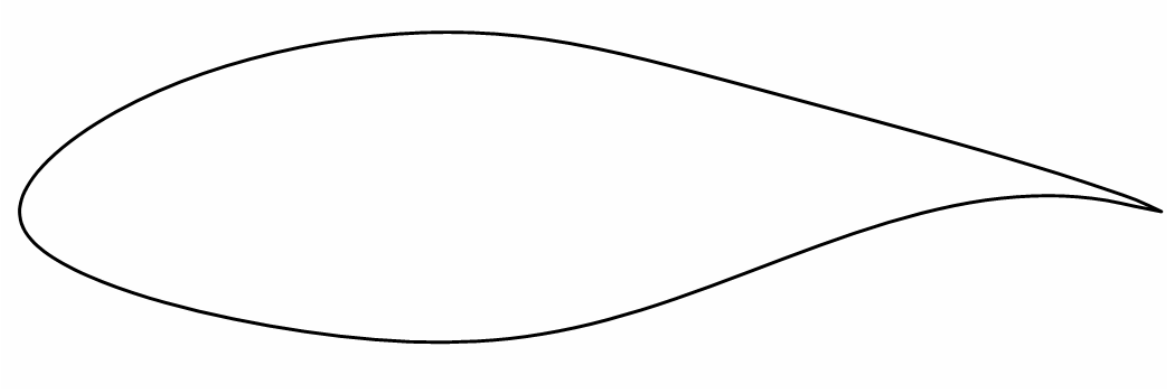

Fig. 32 Airfoil used for LM wind tunnel experiments

Figure 33, Figure 34 present the two setups in the wind tunnel. The model is in aluminum it is split in two parts. The same main part is used for the flap and the mini-flap. Only the trailing edge needs to be change. The mini-flap is attached to the main body by a rubber. The driving system is double and symmetric on the two turn table walls with one master and one slave electric motor. They are mounted outside the turn table walls and are the same for two active devices. The flap is driven by a rotation axis and the mini-flap by forks that are smaller than walls boundary layers.

Pressure taps are distributed along the main body and the flap and mini-flap parts:

- Main body: 81 pressure holes
- Flap: 11 holes
- Mini-flap: 8 holes (there is no pressure measurements on the mini-flap itself)

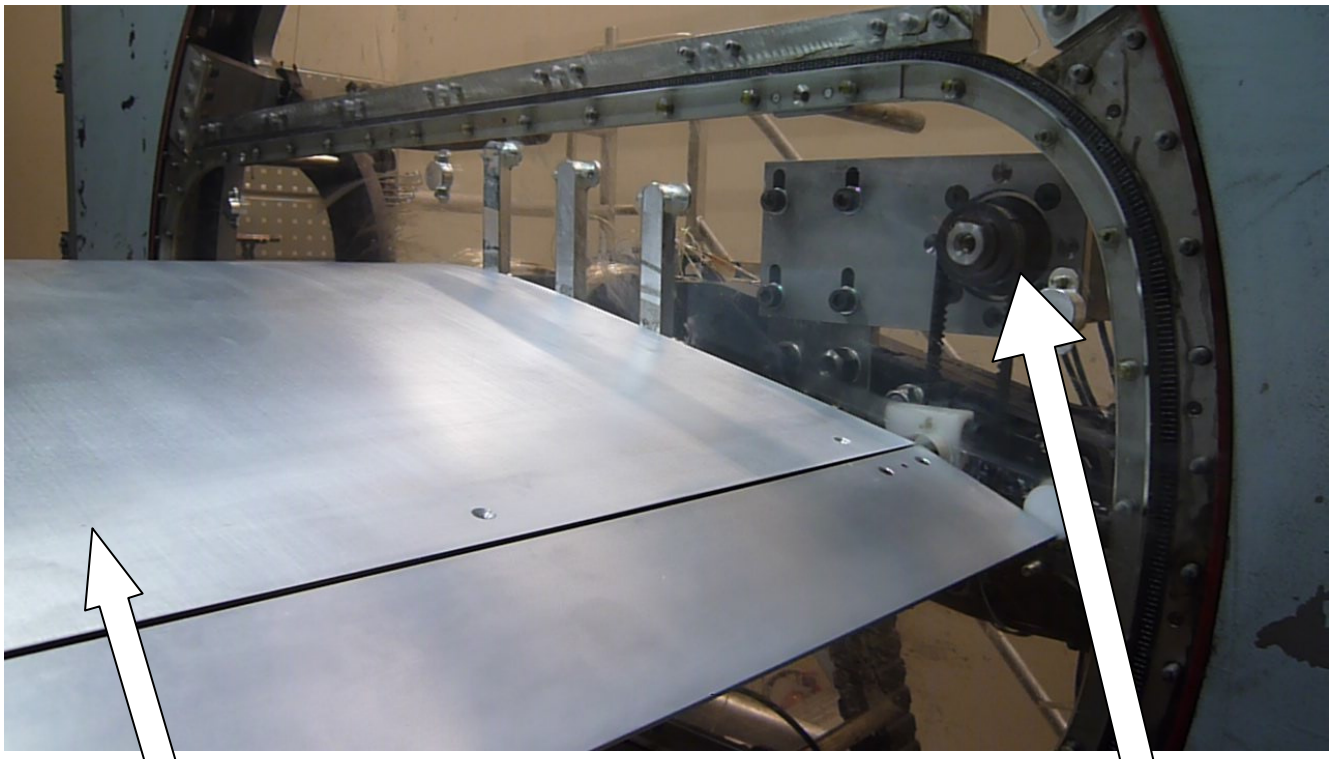

Fig. 33 LM airfoil with Flap (10%C) inched by 10 degree downward

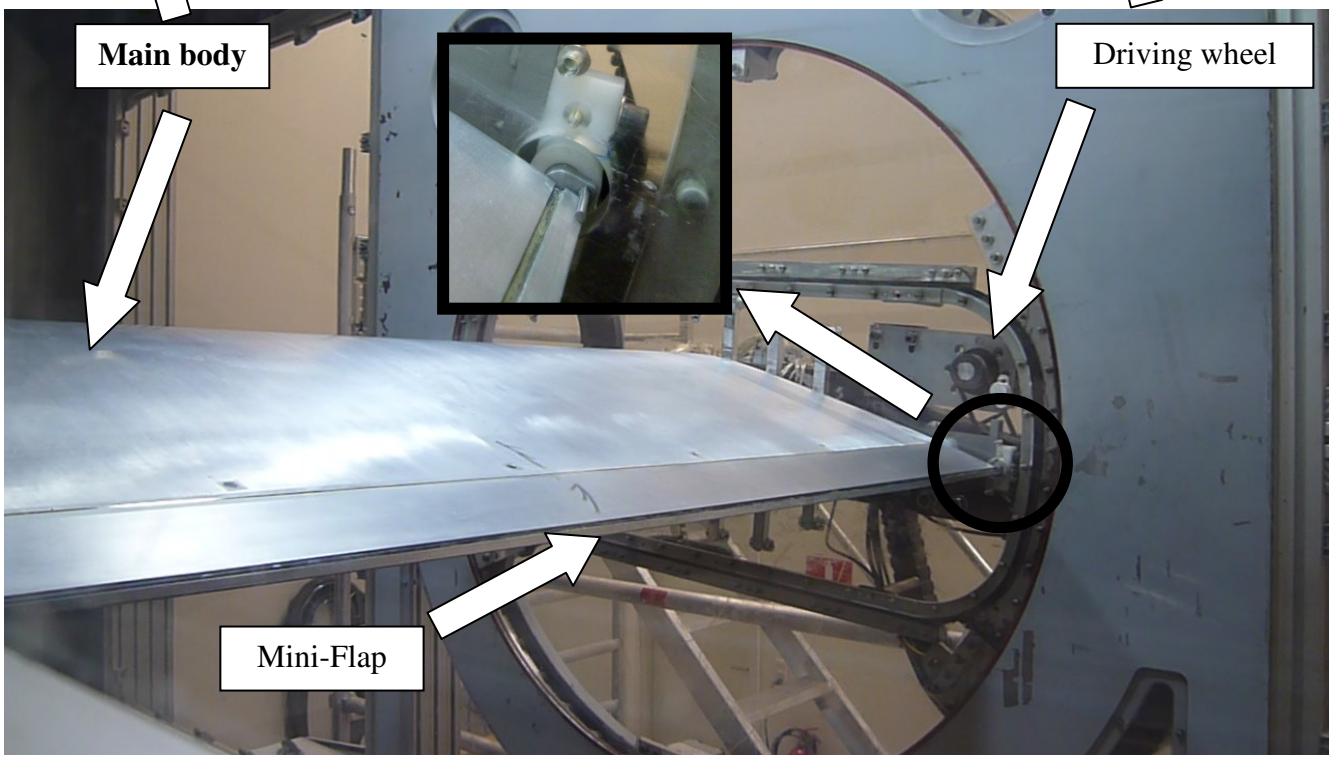

Fig. 34 LM airfoil with Mini-Flap (1%C) inched by 45 degree downward

Steady state polars

Figure 35, Figure 36 presents the steady state results for the flap and the mini-flap at different angle. When the device is flapped down (β positive) the Cl is increased, on the other hand when the device is flapped up (β negative) the Cl is decreased. For the flap, the Cl variation is proportional to the flap angle, for the mini-flap out of the range βϵ [+45,-45], the Cl is not really influence.

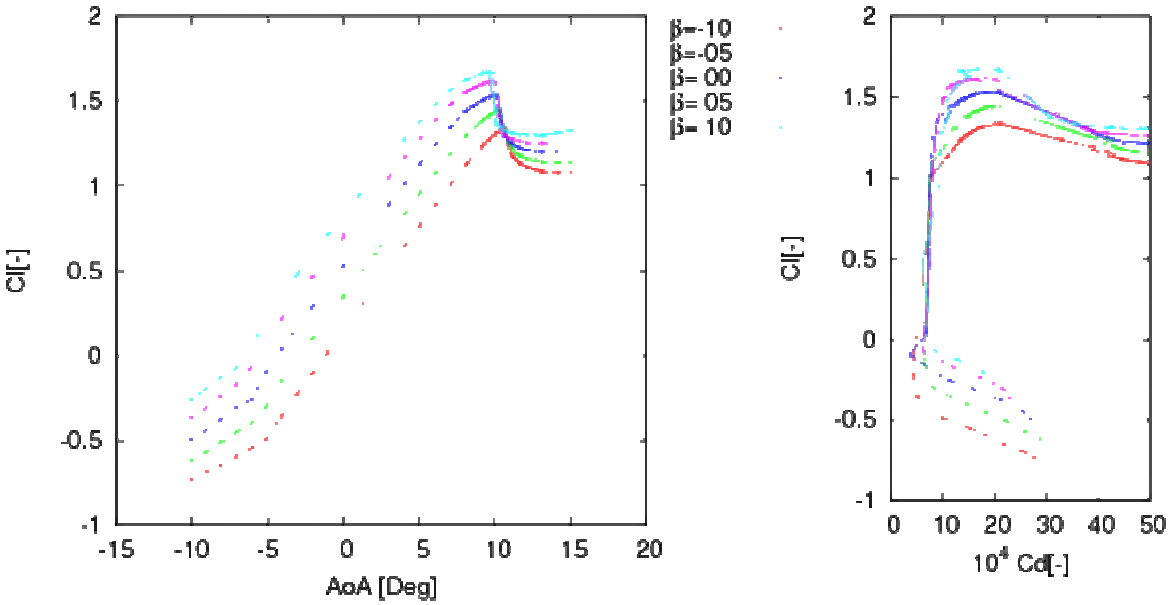

Fig. 35 Steady state polar for flap β= -10, -5, 0, +5 and +10 degree

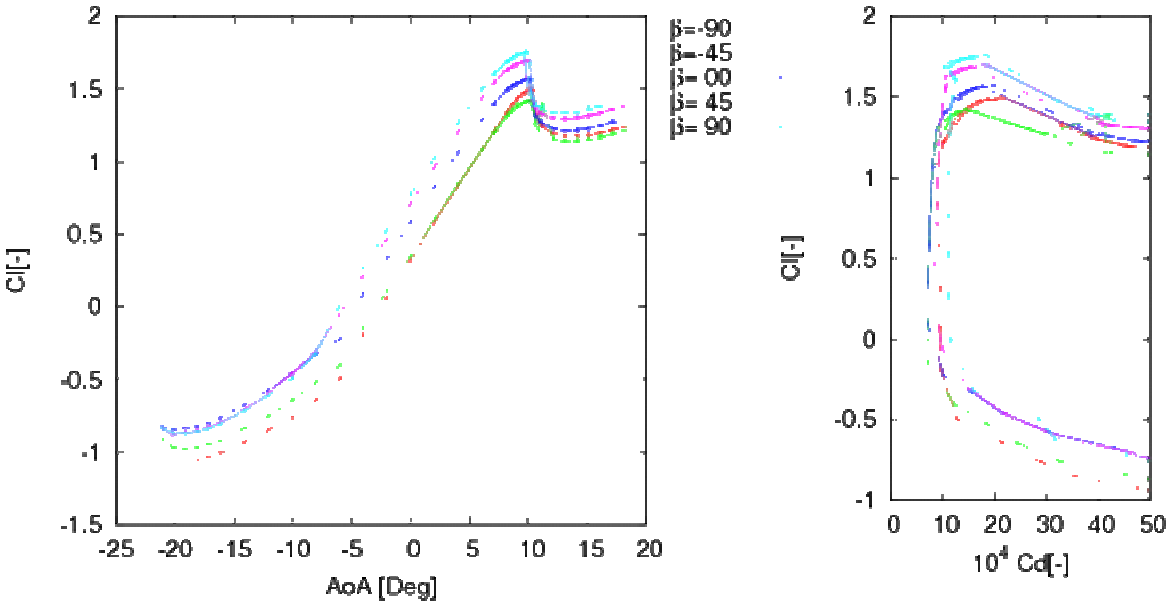

Fig. 36 Steady state polar for mini-flap β= -90, -45, 0, +45 and 90 degree

Example of unsteady Cl polars for flap and mini-flap

Figure 37 and Figure 38 are typical example of results (Cl variation) for sinusoidal motion of the flap and the mini-flap. The results presented in are taken for Re 3000000 at design angle of attack. For the two cases, the reduce frequency k[1]=0.05, k=0.1 and k=0.2 which correspond to a frequency of 0.89, 1.77 and 3.54 Hz with the current wind speed and profile chord.

For the flap case the Cl ellipse are perfectly smooth. The Cl variation range is a little smaller when the frequency is increased. On the other hand, for the mini-flap, the ellipse are not smooth, this is probably due to the rubber part which link the airfoil with the mini-flap. The kink in the surface might create local separation bubble.

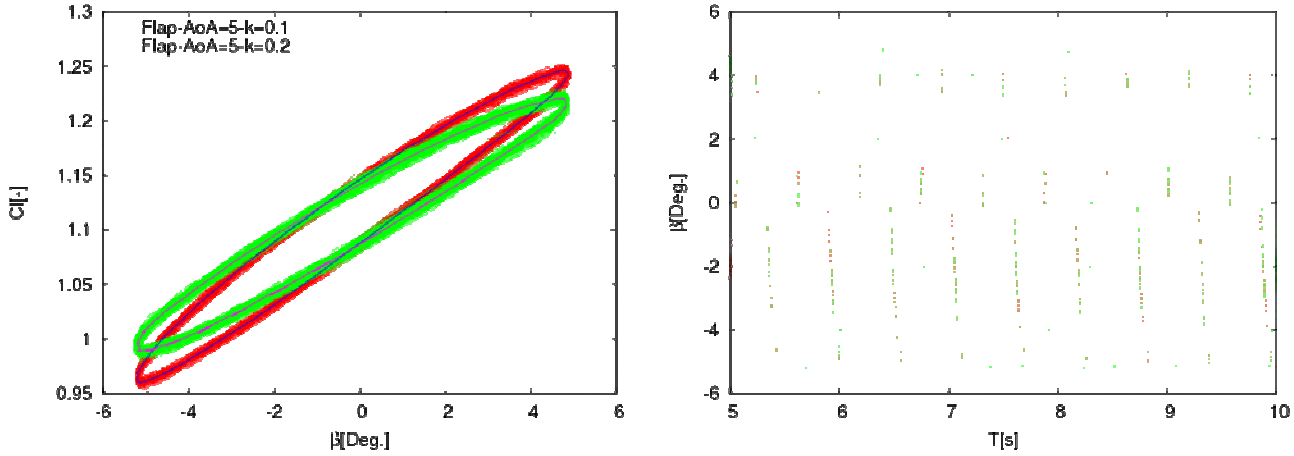

Fig. 37 Flap unsteady Cl for βϵ[+5,-5] at reduce frequency k=0.1 and k=0.2

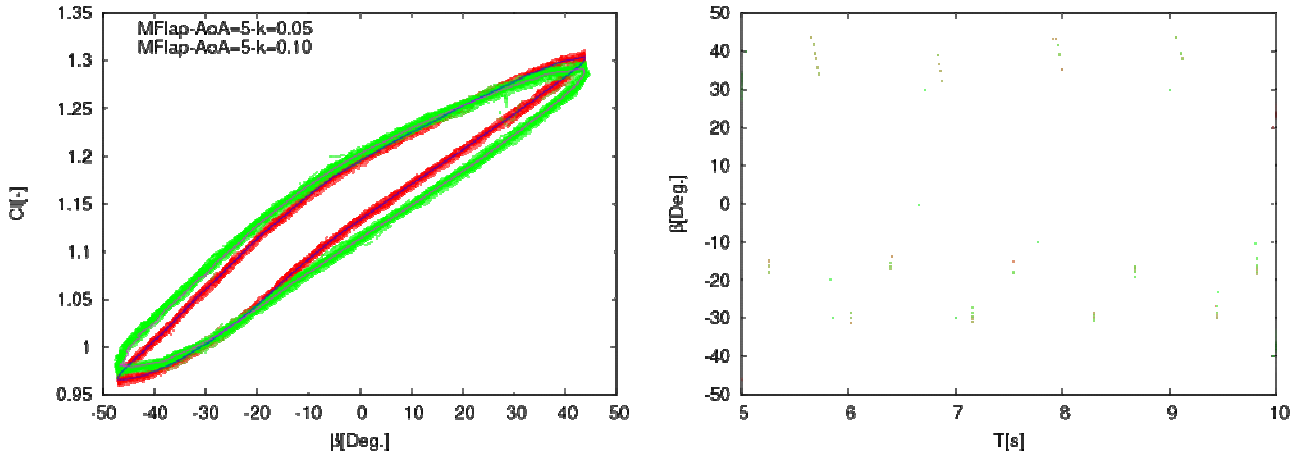

Fig. 38 Mini-Flap unsteady Cl for βϵ[+45,-45] at reduce frequency k=0.05 and k=0.1

[1] $k = \frac{f \bullet \chi}{V}$

6 Bibliography

[Althaus1996] D.Althaus: *„Niedriggeschwindigkeitsprofile“,* ISBN 3-528-03820, Vieweg Verlag Braunschweig/Wiesbaden, 1996.

[Althaus2003-1] D.Althaus: "Tunnel-Wall Corrections at the Laminar Wind Tunnel", Institute report, IAG, http://www.iag.uni-stuttgart.de/laminarwindkanal, December 2003.

[Althaus2003-2] D.Althaus: "Measurement of Lift and Drag in the Laminar Wind Tunnel", Institute report, IAG, http://www.iag.uni-stuttgart.de/laminarwindkanal, December 2003.

[Barlas2009] T.K. Barlas, G.A.M. van Kuik, *“Aeroelastic Modelling and Comparison of Advanced Active Flap Control Concepts for Load Reduction on the Upwind 5MW Wind Turbine“,* Proceedings EWEC 2009, 2009.

[Barlas2008] T.K. Barlas, *“Aerodynamic requirements of NACA 64618 airfoil with control surface“,* UPWIND note, March 2008.

[Barlas2008-2] T.K. Barlas et al., *“Requirements for Smart Rotor Technology Based on the Upwind 5MW reference wind turbine“,* UPWIND report, July 2008.

[Blake1986] Blake, W., Mechanics of Flow Induced Sound and Vibrations. Vols. 1-2 Acad. Press. New-York (1986).

[Chandiramani1974] K. Chandiramani: Diffraction of evanescent wave with application to aerodynamically scattered sound and radiation from unbaffled plates. J. Acoust. Soc. Amer., Vol. 55, 1974.

[Drela89] Drela, M.: *XFOIL: An Analysis and Design System for Low Reynolds Number Airfoils*, Proc. Low Reynolds Number Aerodynamics, June 1989, University of Notre Dame, USA.

[Herrig2005] A. Herrig: SIROCCO. *Trailing edge noise measurements of wind turbine aerofoils in open and closed test section wind tunnels.* Wind Turbine Noise: Perspectives for Control, Berlin, Germany, October 17-18, 2005.

[Herrig2006] A. Herrig, W. Würz, Th. Lutz, E. Krämer: SIROCCO. *Trailing edge noise measurements using a hot-wire based coherent particle velocity method.* 24th Applied Aerodynamics Conference, San Francisco, CA, AIAA Paper 2006-3876, 2006.

[Hulskamp2008] T. Hulskamp (Ed.), *“UPWIND Work Package WP1B3 Year Two Progress Report“,* Delft University of Technology, March 2008.

[Kamruzzaman2007] M. Kamruzzaman, Th. Lutz, E. Krämer: *An Approach to RANS Based Prediction of Airfoil Trailing Edge Far-Field Noise*, Conf. Proc. Wind Turbine Noise, Lyon, France, September 20-21, France, 2007.

[Kamruzzaman2008] M. Kamruzzaman, Th. Lutz, A. Herrig, and E. Krämer: RANS based prediction of airfoil trailing edge far-field noise: Impact of isotropic & anisotropic

turbulence. AIAA Paper 2008-2867-685.

[Kamruzzaman2010-1] M. Kamruzzaman, Th. Lutz, A. Herrig, and E. Krämer. Semi-empirical modeling of turbulent anisotropy for airfoil self noise prediction. AIAA Paper 2010-3878.

[Kamruzzaman2010-2] M. Kamruzzaman, Th. Lutz, W. Würz, W. Shen, W. J. Zhu, M. Hansen, F. Bertagnolio, and H. Madsen: Validations and improvements of aeroacoustic models using detailed experimental data, submitted to J. of Wind Energy, July 2010.

[Kamruzzaman2010-3] M. Kamruzzaman, Th. Lutz and E. Krämer: Improved Wind Turbine Noise Prediction Tools for Low Noise Airfoil Design, DEWEK, 17-18 November, Bremen, Germany, 2010.

[Kamruzzaman2011] Kamruzzaman, M.; Herrig, A.; Lutz, Th.; Würz, W.; Krämer, E.; Wagner, S.: *"Comprehensive evaluation and assessment of trailing edge noise prediction based on dedicated measurements",* Int. J. of Noise Control Eng., 2-2011.

[Kroll2010] N. Kroll, C.C. Rossow, D. Schwamborn, K. Becker: *MEGAFLOW - A Numerical Flow Simulation Tool for Transport Aircraft Design*, Proceedings of the 23rd International Congress of Aeronautical Sciences ICAS, 2002, Toronto.

[Lackner2009] M.A. Lackner, G.A.M. van Kuik, *"A Comparison of Smart Rotor Control Approaches using Trailing Edge Flaps and Individual Pitch Control",* AIAA paper 2009-685, 47th AIAA Aerospace Sciences Meeting, 5-8 January 2009, Orlando, Florida, USA, 2009.

[Langen2007] P. van Langen, *"UpWind reference wind turbine version 8",* UPWIND note, 21 February 2007.

[Lutz2004] *Airfoil Sections.* DEWEK 2004, 7th German wind energy conference, Wilhelmshaven, October 20-21, 2004.

[Lutz2005] Th. Lutz, A. Herrig, W. Würz, K. Braun, E. Krämer: *Constrained Aerodynamic & Aeroacoustic Design of Wind-Rotor.* Wind Turbine Noise: Perspectives for Control, Berlin, Germany, October 17-18, 2005.

[Lutz2006] Th. Lutz, W. Würz, A. Herrig, K. Braun, E. Krämer, J.G. Schepers, A.P.W.M. Curvers, S. Oerlemans, A. Matesanz, R. Ahrelt, T. Maeder, S. Herr: *New Results from the European SIROCCO Project: Silent Rotors by Acoustic Optimization.* DEWEK 2006, 8th German wind energy conference, Bremen, Germany, November 26-27, 2006.

[Lutz2007] Th. Lutz, A. Herrig, W. Würz, M. Kamruzzaman, E. Krämer: *Design and Wind-Tunnel Verification of Low-Noise Airfoils for Wind Turbines.* AIAA Journal, Vol. 45, No. 4, April 2007, pp. 779-785.

[Lutz2007-2] Th. Lutz: UPWIND Work Package 1B3: *Boundary Layer Analyses of the Flapped NACA 64-418 and DU96W180 Airfoils,* Internal Report, Institute of Aerodynamics and Gas Dynamics, University of Stuttgart, 1 August 2007.

[Lutz2007-3] Th. Lutz: UPWIND Work Package 1B3: *Aerodynamic & aeroacoustic design and verification of an adaptive airfoil with trailing-edge flap,* UPWIND progress report, Institute of Aerodynamics and Gas Dynamics, University of Stuttgart, September 2007.

[Lutz2010] Th. Lutz and A. Wolf: Aerodynamic and Acoustic Design of Wind Turbine Airfoils with Trailing-Edge Flap, DEWEK, 17-18 November, Bremen, Germany, 2010.

[Meister2009] Meister, K.; Lutz, Th.; Krämer, E.: *"Development of a process chain for detailed wake simulation of horizontal axis wind turbines"*, EUROMECH [508] - Wind turbine wakes, Madrid, October 20-22, 2009.

[Meister2010] Meister, K.; Lutz, Th.; Krämer, E.: *"Consideration of unsteady inflow conditions in wind turbine CFD simulations"*, Proc. DEWEK 2010.

[Parchen1998] R. Parchen. Progress report DRAW, a prediction scheme for trailing-edge noise based on detailed boundary-layer characteristics. TNO-report HAG-RPT-980023, The Netherlands, 1998.

[Troldborg2005] N. Troldborg, *"Computational study of the Risø-B1-18 airfoil with a hinged flap providing variable trailing-edge geometry"*, Wind Engineering, Vol. 29, No. 2, 2005.

[Wilcox1998] David C. Wilcox. Turbulence Modeling for CFD. DCW Industries, Inc., 2nd edition, 1998.

[Wolf2009] A. Wolf, M. Kamruzzaman, W. Würz, Th. Lutz, E. Krämer: *"Wall pressure fluctuation (WPF) and trailing-edge noise measurements on a NACA 64_3-418 airfoil"*, Internal technical report, Institute of Aerodynamics and Gas Dynamics, University of Stuttgart, January 2008.

[Wolf2010] A. Wolf, M. Kamruzzaman, W. Würz, Th. Lutz, E. Krämer: *"Aerodynamic and aeroacoustic measurements on the TL 190-82 airfoil with 10% trailing-edge"*, Internal technical report, Institute of Aerodynamics and Gas Dynamics, University of Stuttgart, December 2010.

[Wolf2010-2] A. Wolf: *"Survey on flow control devices for load control and performance improvement"*, Internal technical report, Institute of Aerodynamics and Gas Dynamics, University of Stuttgart, December 2010.

[Würz2004] W. Würz, S. Guidati, A. Herrig, Th. Lutz, S. Wagner: *Measurement of trailing edge noise by a coherent particle velocity method.* Proc. ICMAR, Novosibirsk, June 28 –July, 2004.

[Würz2008] W. Würz, A. Herrig, M. Kamruzzaman, A. Ivanov: *"Measurements of normal-to-wall and spanwise integral correlation lengths at the trailing edge of the NACA 64_3-418"*, Internal technical report, Institute of Aerodynamics and Gas Dynamics, University of Stuttgart, January 2008.